Article

Immunity

Leveraging vaccination-induced protective antibodies to define conserved epitopes on influenza N2 neuraminidase

Graphical abstract

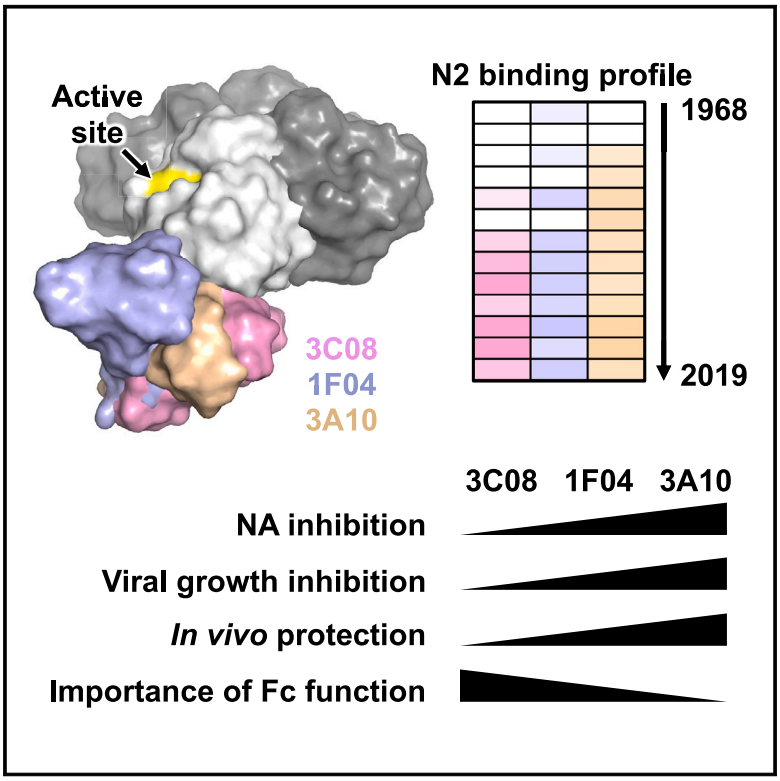

Highlights

- Cryo-EM structures of three clonally distinct NA antibodies (Abs)
- NA Abs bind to overlapping conserved epitopes in the underside of NA head domain
- Ab epitopes have minimal overlap with other structurally defined NA epitopes
- The defined NA Abs inhibit NA activity and confer protection *in vivo*

Authors

Ruipeng Lei, Wooseob Kim, Huibin Lv, ..., Xinghong Dai, Ali H. Ellebedy, Nicholas C. Wu

Correspondence

kapunmok@cuhk.edu.hk (C.K.P.M.), florian.krammer@mssm.edu (F.K.), xxd159@case.edu (X.D.), ellebedy@wustl.edu (A.H.E.), nicwu@illinois.edu (N.C.W.)

In brief

The immunization potential of antibodies against influenza neuraminidase has been underappreciated. Here, Lei et al. isolated three protective antibodies that cross-react with neuraminidases from seasonal H3N2 strains spanning multiple decades. Structural and functional characterization provides insights into antibody response against influenza neuraminidase with implications for developing broadly protective influenza vaccines.

Lei et al., 2023, Immunity *56*, 2621–2634
November 14, 2023
https://doi.org/10.1016/j.immuni.2023.10.005

CellPress

Immunity

CellPress

Article

Leveraging vaccination-induced protective antibodies to define conserved epitopes on influenza N2 neuraminidase

Ruipeng Lei,[1,19] Wooseob Kim,[2,3,19] Huibin Lv,[1,4,19] Zongjun Mou,[5,19] Michael J. Scherm,[6,19] Aaron J. Schmitz,[2] Jackson S. Turner,[2] Timothy J.C. Tan,[7] Yiquan Wang,[1] Wenhao O. Ouyang,[1] Weiwen Liang,[4] Joel Rivera-Cardona,[8] Chuyun Teo,[1] Claire S. Graham,[1] Christopher B. Brooke,[8] Rachel M. Presti,[9,10,11] Chris K.P. Mok,[12,13,14,*] Florian Krammer,[6,15,16,*] Xinghong Dai,[5,*] Ali H. Ellebedy,[2,10,11,*] and Nicholas C. Wu[1,7,17,18,20,*]

[1]Department of Biochemistry, University of Illinois at Urbana-Champaign, Urbana, IL 61801, USA
[2]Department of Pathology and Immunology, Washington University School of Medicine, Saint Louis, MO 63110, USA
[3]Department of Microbiology, Korea University College of Medicine, Seoul 02841, Korea
[4]HKU-Pasteur Research Pole, School of Public Health, Li Ka Shing Faculty of Medicine, The University of Hong Kong, Hong Kong SAR, China
[5]Department of Physiology and Biophysics, Case Western Reserve University, Cleveland, OH 44106, USA
[6]Department of Microbiology, Icahn School of Medicine at Mount Sinai, New York, NY 10029, USA
[7]Center for Biophysics and Quantitative Biology, University of Illinois at Urbana-Champaign, Urbana, IL 61801, USA
[8]Department of Microbiology, University of Illinois at Urbana-Champaign, Urbana, IL 61801, USA
[9]Division of Infectious Diseases, Department of Medicine, Washington University School of Medicine, Saint Louis, MO 63110, USA
[10]Center for Vaccines and Immunity to Microbial Pathogens, Washington University School of Medicine, Saint Louis, MO 63110, USA
[11]The Andrew M. and Jane M. Bursky Center for Human Immunology and Immunotherapy Programs, Washington University School of Medicine, Saint Louis, MO 63110, USA
[12]The Jockey Club School of Public Health and Primary Care, The Chinese University of Hong Kong, Hong Kong SAR, China
[13]Li Ka Shing Institute of Health Sciences, Faculty of Medicine, The Chinese University of Hong Kong, Hong Kong SAR, China
[14]S.H. Ho Research Centre for Infectious Diseases, The Chinese University of Hong Kong, Hong Kong SAR, China
[15]Department of Pathology, Molecular and Cell Based Medicine, Icahn School of Medicine at Mount Sinai, New York, NY 10029, USA
[16]Center for Vaccine Research and Pandemic Preparedness (C-VARPP), Icahn School of Medicine at Mount Sinai, New York, NY 10029, USA
[17]Carl R. Woese Institute for Genomic Biology, University of Illinois at Urbana-Champaign, Urbana, IL 61801, USA
[18]Carle Illinois College of Medicine, University of Illinois at Urbana-Champaign, Urbana, IL 61801, USA
[19]These authors contributed equally
[20]Lead contact
*Correspondence: kapunmok@cuhk.edu.hk (C.K.P.M.), florian.krammer@mssm.edu (F.K.), xxd159@case.edu (X.D.), ellebedy@wustl.edu (A. H.E.), nicwu@illinois.edu (N.C.W.)
https://doi.org/10.1016/j.immuni.2023.10.005

SUMMARY

There is growing appreciation for neuraminidase (NA) as an influenza vaccine target; however, its antigenicity remains poorly characterized. In this study, we isolated three broadly reactive N2 antibodies from the plasmablasts of a single vaccinee, including one that cross-reacts with NAs from seasonal H3N2 strains spanning five decades. Although these three antibodies have diverse germline usages, they recognize similar epitopes that are distant from the NA active site and instead involve the highly conserved underside of NA head domain. We also showed that all three antibodies confer prophylactic and therapeutic protection *in vivo*, due to both Fc effector functions and NA inhibition through steric hindrance. Additionally, the contribution of Fc effector functions to protection *in vivo* inversely correlates with viral growth inhibition activity *in vitro*. Overall, our findings advance the understanding of NA antibody response and provide important insights into the development of a broadly protective influenza vaccine.

INTRODUCTION

Due to the practice of masking and social distancing during the coronavirus disease 2019 (COVID-19) pandemic, the activity of human influenza A virus was extremely low throughout the 2020–2021 influenza season.[1] However, the activity of human influenza A virus, especially the H3N2 subtype, increased substantially in the 2021–2022 influenza season,[2] demonstrating its persistence in the human population. In fact, H3N2 virus has been circulating in humans for more than half a century since the 1968 Hong Kong influenza pandemic. Seasonal influenza vaccination is currently the major countermeasure against human influenza virus infection. Although there are two major antigens on influenza A virus, hemagglutinin (HA) and neuraminidase (NA), influenza vaccine development has largely focused on HA. Nevertheless, studies show that the NA antibody response represents a correlate of protection that is independent of HA antibody response.[3–7] Given that the current seasonal influenza

Table 1. Binding affinity against recombinant NAs from different influenza strains

Subtype	Strain	1F04 Fab (K_D)	3C08 Fab (K_D)	3A10 Fab (K_D)
H3N2	A/Hong Kong/1/1968	125 nM	no binding	no binding
H3N2	A/Bilthoven/17938/1969	no binding	no binding	no binding
H3N2	A/Bilthoven/21438/1971	134 nM	no binding	26 nM
H3N2	A/Albany/1/1976	no binding	no binding	13 nM
H3N2	A/Bangkok/1/1979	12 nM	133 nM	3 nM
H3N2	A/Beijing/353/1989	no binding	no binding	3 nM
H3N2	A/Shandong/9/1993	10 nM	25 nM	7 nM
H3N2	A/Moscow/10/1999	8 nM	4 nM	8 nM
H3N2	A/Wyoming/3/2003	7 nM	<1 nM	13 nM
H3N2	A/Victoria/361/2011	15 nM	23 nM	6 nM
H3N2	A/Singapore/INFIMH-16-0019/2016	3 nM	<1 nM	<1 nM
H3N2	A/Kansas/14/2017	26 nM	<1 nM	<1 nM
H3N2	A/Hong Kong/2671/2019	6 nM	10 nM	6 nM
H2N2	A/Canada/720/2005	no binding	no binding	no binding
H5N2	A/mallard/Netherlands/3/1999	no binding	no binding	no binding
H9N2	A/quail/Hong Kong/G1/1997	no binding	no binding	455 nM

See also Figures S1 and S3.

vaccines offer suboptimal protection, NA is receiving increased attention for influenza vaccine development.[8,9] Despite the importance of NA in public health, molecular understanding of NA antibody response is severely lacking compared with HA antibody response.

NA is a homotetrameric glycoprotein that cleaves the sialylated glycan to promote virus release.[10] When the first NA structure was determined in 1983,[11] seven antigenic regions at the rim of the catalytic site were proposed to be targeted by antibodies.[12] However, as more NA-antibody complex structures are determined,[13–20] it becomes clear that residues outside of the classical antigenic regions can also be targeted by antibodies. Notably, several antibodies that bind to the highly conserved NA active site have been identified.[16–19,21] These active site-targeting antibodies are protective and can cross-react with multiple strains within a given NA subtype[16,22] or even across different NA subtypes.[17,18,21] As a result, NA can potentially contribute to the development of a universal influenza vaccine, which is a priority for the National Institute of Allergy and Infectious Diseases.[23]

In this study, we isolated three vaccination-induced NA antibodies from a single individual. These antibodies cross-reacted with the NAs from multiple seasonal influenza H3N2 strains. The one with the highest binding breadth, 3A10, also cross-reacted with the NA from an H9N2 strain. Cryoelectron microscopy (cryo-EM) analysis showed that the epitopes of these antibodies highly overlapped and involved the underside of NA head domain, which is highly conserved. Nevertheless, the binding modes and germline usages of these three antibodies were very different. Although their epitopes were far from the active site, two of the three antibodies inhibited viral growth, likely by preventing the NA to access its substrate on the cell surface. Furthermore, all three antibodies, including the one that did not inhibit viral growth *in vitro*, showed *in vivo* protection activity.

RESULTS

Three broadly reactive N2 antibodies from a single donor

We isolated 10 monoclonal antibodies to NA and 24 to HA from the plasmablasts of an individual 1 week after receiving the Flucelvax vaccine (a cell-based vaccine) during the 2019–2020 influenza season. This individual was also previously studied after vaccination with the Flucelvax vaccine during the 2018–2019 influenza season.[24] Here, we focused on three of these NA antibodies, namely, 3C08, 3A10, and 1F04 (Figure S1), which were encoded by IGHV4-59/IGLV1-44, IGHV4-30-4/IGLV1-40, and IGHV3-48/IGKV3-20, respectively (Figure S2). Although all three N2 antibodies cross-reacted with multiple N2 NAs, 3A10 had the highest binding breadth among them (Table 1; Figure S3). 3A10 had reasonable binding affinity (K_D < 30 nM) to NAs from human H3N2 strains spanning from 1971 to 2019 (49 years). In addition, 3A10 also bound to the NA from an H9N2 strain, albeit with a low affinity (K_D = 455 nM). These results indicate that the epitopes of 3C08, 3A10, and 1F04 are relatively conserved on N2 NA.

All three antibodies bind to the underside of NA head domain

To understand how 3C08, 3A10, and 1F04 bind to NA, we determined the cryo-EM structures of A/Moscow/10/1999 (Mos99) NA in complex with 3C08, 3A10, and 1F04 at resolutions of 2.78, 2.50, and 2.63 Å, respectively (Figure S4; Table S1). Our structural analysis showed that these three antibodies bound to a similar region on NA that involved the underside of NA head domain and was distant from the active site (Figures 1A–1C). In fact, 3C08 and 3A10 shared an almost identical epitope (Figures 1D and 1E) despite the huge disparity in their relative positioning of heavy and light chains with respect to NA (Figures 1A and 1B). In comparison, the epitope of 1F04 shifted slightly toward the active site (Figure 1F). The epitopes of 3C08,

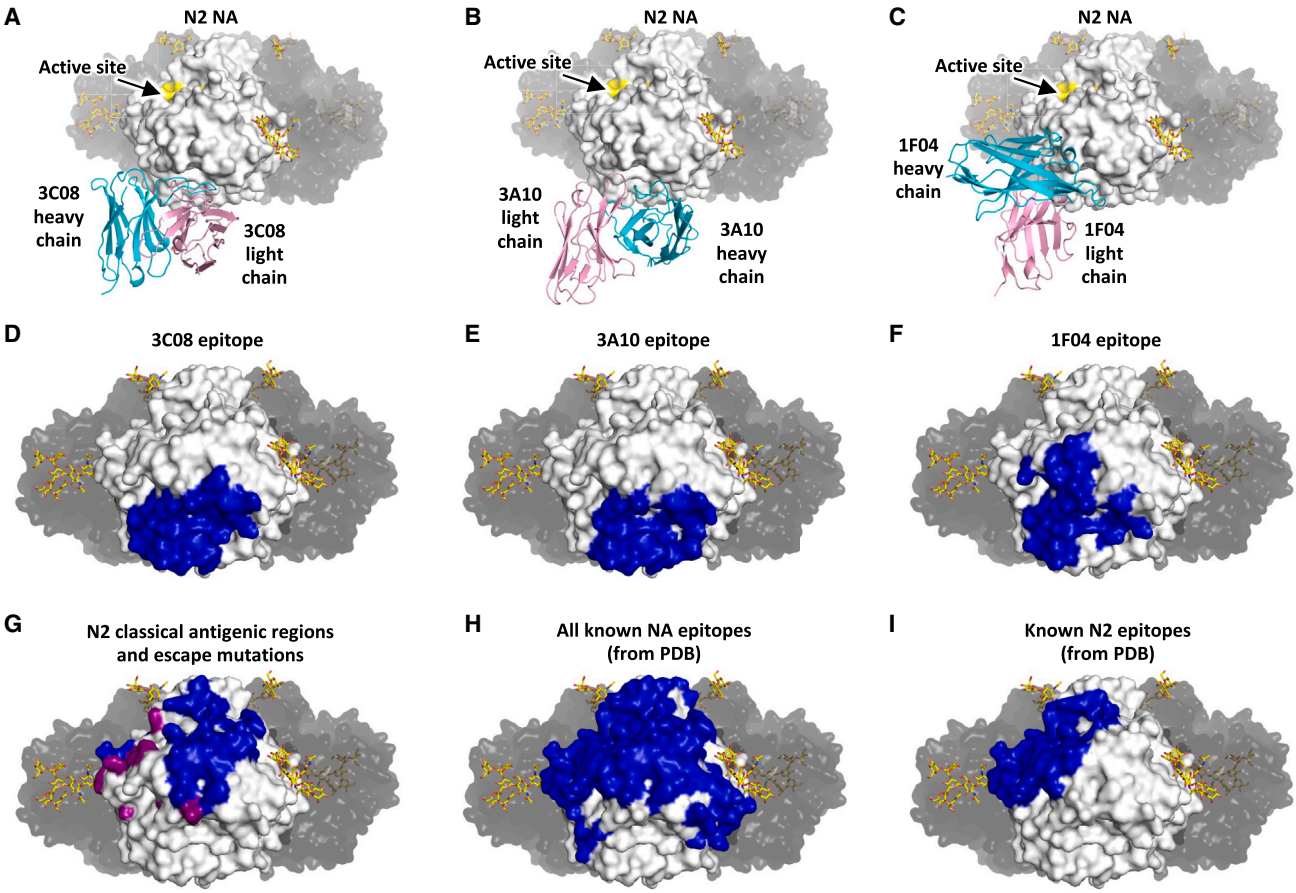

Figure 1. Structural characterization of the three antibodies to the underside of NA head domain

(A–C) Cryo-EM structures of Mos99 NA in complex with (A) 3C08 Fab, (B) 3A10 Fab, and (C) 1F04 Fab. For clarity, only the variable region of one Fab is displayed in each tetrameric structure. The NA is in surface representation with one protomer colored in white and the other three in dark gray. The active site of NA is highlighted in yellow. The heavy chain of each antibody is colored in cyan and light chain in pink. Glycans are shown as sticks.

(D–F) The epitopes of (D) 3C08, (E) 3A10, and (F) 1F04 are highlighted in blue on the NA structure.

(G) The locations of classical antigenic regions of N2 NA (blue)[12] as well as known antibody escape mutations in N2 NA from eight studies that are outside of the classical antigenic regions (purple).[15,25–31]

(H) The epitopes of NA antibodies (any influenza A subtype or type B) with structural information available in PDB.

(I) The epitopes of all N2 NA antibodies in PDB. In all panels, Mos99 NA structure (PDB: 7U4F) is used.[32]

See also Figure S4 and Tables S1–S3.

3A10, and 1F04 had minimal overlap with the classical antigenic regions of N2 NA[11] as well as the locations of known N2 antibody escape mutations that we compiled from eight studies (Figure 1G; Table S2).[15,25–31] A previously identified N2 antibody escape mutation, E258K, locates at the underside of NA[28] but is outside of the epitopes of 3C08, 3A10, and 1F04. In addition, none of the 16 NA antibodies with structural information available in Protein Data Bank (PDB) target the same epitopes as 3C08, 3A10, and 1F04 (Figures 1H and 1I; Table S3). As a result, little is known regarding the epitopes of 3C08, 3A10, and 1F04.

3C08, 1F04, and 3A10 have diverse binding modes to highly overlapping epitopes

We next examined the structural features of 3C08, 3A10, and 1F04. In 3C08, the 17-amino acid complementarity-determining region (CDR) H3 (Kabat numbering), which bent toward the light chain and formed extensive interaction with NA (Figure 2A), accounted for 56% of the buried surface area (BSA) of the paratope. 3C08 used V_H L99 and V_H W100a in the CDR H3 to fill two pockets in the underside of NA head domain (Figure 2B). Moreover, CDR H3 of 3C08 also formed four H-bonds with NA using the side chains of V_H R100, V_H S100c, and V_H R100d, as well as the main chain of V_H W100a (Figure 2C). Although 3C08 also used other CDRs for binding (Figures S2A and S2B), none of its NA-interacting side chains represented somatic hypermutation (SHM) (Figures S5A–S5C).

Unlike 3C08, 3A10 primarily used CDR H2 for binding, which accounted for 40% of the BSA of the paratope (Figures 2D and S5D–S5F). The CDR H2 of 3A10 formed three H-bonds with NA using the side chains of V_H N52 and V_H N56, as well as the main chain of V_H A57 (Figure 2E). In addition, V_H F58 in the CDR H2 of 3A10 participated in a cation-π interaction with NA. Half of the residues in the CDR H2 of 3A10 were SHMs, most of which were in the paratope (Figures 2E and S2D). To

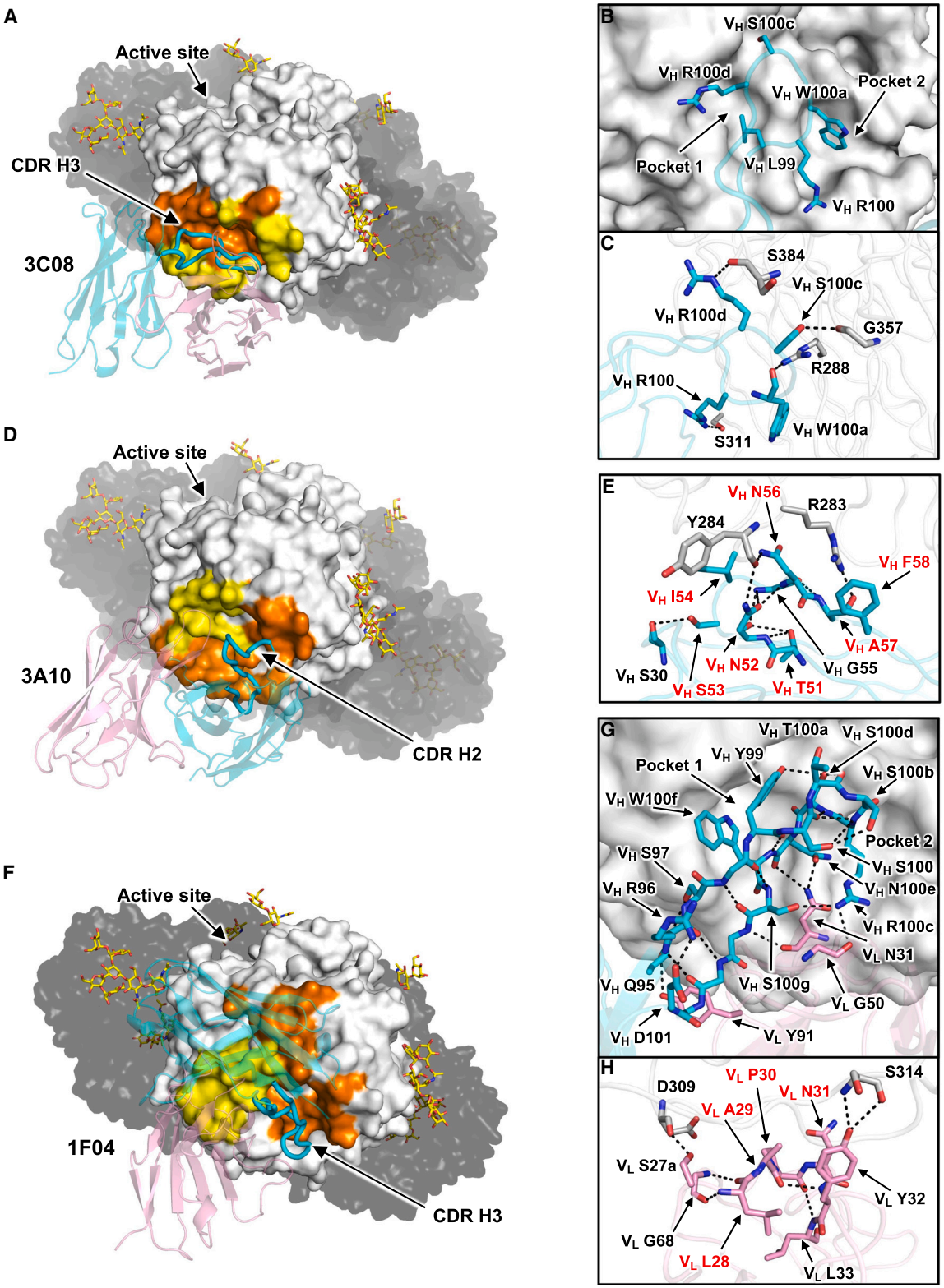

Figure 2. Atomic interactions between NA and the three antibodies

(A) Interactions between 3C08 and NA.

(B and C) Two pockets on NA surface that are occupied by the CDR H3 of 3C08 are indicated. Key CDR H3 residues of 3C08 that interact with NA are shown.

(D) Interactions between 3A10 and NA.

(legend continued on next page)

understand the importance of SHMs in binding, two CDR H2 mutants of 3A10 were constructed. Although mutant 1, which consisted of germline reversions V_H N52Y, V_H S53Y, and V_H I54S, did not affect the binding to Mos99 NA, mutant 2, which consisted of germline mutations V_H N56S, V_H A57T, and V_H F58Y, dramatically weakened the binding (Figure S6A). This result showed that SHMs in 3A10 were critical for NA binding. The very different binding modes between 3C08 and 3A10 help explain their differences in binding breadth (Table 1), despite having highly similar binding footprints on NA (Figures 1D and 1E).

Similar to 3C08, 1F04 heavily relied on an 18-amino acid CDR H3 (Kabat numbering) for binding, which accounted for 44% of the BSA of the paratope (Figure 2F). The CDR H3 of 1F04 formed a β-hairpin with an α-turn, which stabilized its conformation via many intramolecular backbone H-bonds (Figure 2G). The conformational stability of the CDR H3 was further augmented by additional intramolecular H-bonds between the side chains of V_H Y99 and V_H S100d, V_H S100 and V_H S100b, as well as V_H R100c and V_H S100g. Besides, V_H R100c, which located at the tip of the CDR H3, helped anchor the CDR H3 by forming an H-bond with the backbone of V_L G50 in the CDR L2 (Figure 2G). The tip of the CDR H3 also interacted with NA via four H-bonds (Figure S5G). Furthermore, the CDR H3 formed another three H-bonds with V_L N31 in the CDR L1 for anchoring (Figure 2G). Through rigidifying the conformation of CDR H3, this huge network of H-bonds would reduce the entropic cost of binding. Two clusters of SHMs were present in the paratope of 1F04—one in the CDR H2 (Figure S5H) and the other in the CDR L1 (Figure 2H). Although germline reversion of CDR H2 did not affect binding to Mos99 NA, that of CDR L1 abolished binding. This result demonstrated the importance of SHMs in 1F04 for NA binding (Figure S6B). Given the drastic differences in binding modes and germline usages among 3C08, 3A10, and 1F04, our analyses indicate that the underside of NA head domain can elicit a diverse antibody response. Nevertheless, because the epitopes involving the underside of NA are close to the stalk domain, antibodies to these epitopes should have a restricted angle of approach (Figures S6C–S6E).

Underside epitopes are highly conserved among human H3N2 NA

To understand the molecular basis of the cross-reactivity of 3C08, 3A10, and 1F04 (Table 1), the sequence conservations of their epitopes were examined. The cores of 3C08, 3A10, and 1F04 epitopes were largely conserved among human H3N2 NAs, whereas a handful of residues at the edge of the epitopes were less conserved (Figures 3A–3C). Consistently, most epitope residues with a large BSA upon binding were highly conserved, including those that were shared among antibodies, such as R283, P285, D309, S311, and S384. Moreover, all epitope residues with side chains that H-bond with the three antibodies had minimal natural variation (Figures 3E–3G). In contrast, the classical antigenic regions[12] were significantly less conserved ($p \leq 0.005$, two-sided Wilcoxon rank-sum test) (Figures 3D and 3H).

Nevertheless, major natural amino acid variants could be observed in a limited number of key epitope residues, as exemplified by residue 313, which had a large BSA upon binding to all three antibodies. NA residue 313 had a Val in human H3N2 strains that were isolated in the past four decades but had an Asp in older human H3N2 strains, as well as A/Canada/720/2005 (H2N2), A/mallard/Netherlands/3/1999 (H5N2), and A/quail/Hong Kong/G1/1997 (H9N2), which were non-seasonal N2 strains (Table S4). Based on our cryo-EM structures, V313 in Mos99 NA closely packed against 3C08, 3A10, and 1F04 upon binding (Figures S5I–S5K). Replacing the hydrophobic Val at residue 313 with Asp, which was a larger and negatively charged amino acid, would increase steric hindrance and hence decrease antibody binding affinity. This observation could at least partially explain the much weaker binding of 3C08, 3A10, and 1F04 to older human H3N2 strains, as well as non-seasonal N2 strains. Consequently, although the epitopes of 3C08, 3A10, and 1F04 were highly conserved, certain natural amino acid variants in N2 strains could reduce or even abolish their binding activity.

We acknowledge that the amino acid sequence at NA residue 313 could not fully explain the variation in binding affinity of these antibodies. For example, A/Beijing/353/1989 (Bei89) NA had a V313 but no detectable binding to 3C08 and 1F04 (Table 1; Figure S3). This observation suggested that the binding activity of antibodies to the underside of NA head domain was also affected by natural mutations at other residues. We then compared the amino acid sequences between Bei89, which had no detectable binding to 3C08, and A/Shandong/9/1993 (SD93), which showed decent binding activity to 3C08 (K_D = 25 nM) (Table 1; Figure S3). In the 3C08 epitope, Bei89 NA and SD93 NA differed by two amino acid mutations, namely, D358N and T385K. Based on our structure of 3C08 in complex with Mos99 NA, the side chain of K385 pointed away from 3C08 and that of N358 only had weak van der Waals interaction with 3C08 (Figure S5L). Thus, mutation T385K would not affect 3C08 binding, whereas the conserved mutation D358N would minimally impact the interaction between NA and 3C08. This analysis indicated that the huge difference in 3C08 binding affinity between Bei89 and SD93 could not be explained by their difference of amino acid sequence in the epitope.

Similarly, in the 1F04 epitope, Bei89 NA and SD93 NA only differed by the conserved mutation D358N. As indicated by our structure of 1F04 in complex with Mos99 NA, N358 formed a polar-polar interaction with 1F04 V_H T100a (Figure S5M). Substituting N358 for D358 would convert the polar-polar interaction into a polar-charge interaction, which should strengthen the binding.

(E) Key CDR H2 residues of 3A10 that interact with NA are shown.
(F) Interactions between 1F04 and NA.
(G) Key CDR H3 residues of 1F04 that interact with NA are shown. Light chain residues that interact with CDR H3 are also shown.
(H) Key CDR L1 residues of 1F04 that interact with NA are shown. In (A), (D), and (F), epitope residues interacting with the heavy chain are shown in orange, whereas those interacting with the light chain are shown in yellow. Other settings are the same as Figures 1A–1C. In all other panels, black dashed lines represent H-bonds. Residues labeled in red represent somatic hypermutations.
See also Figures S2, S5, and S6.

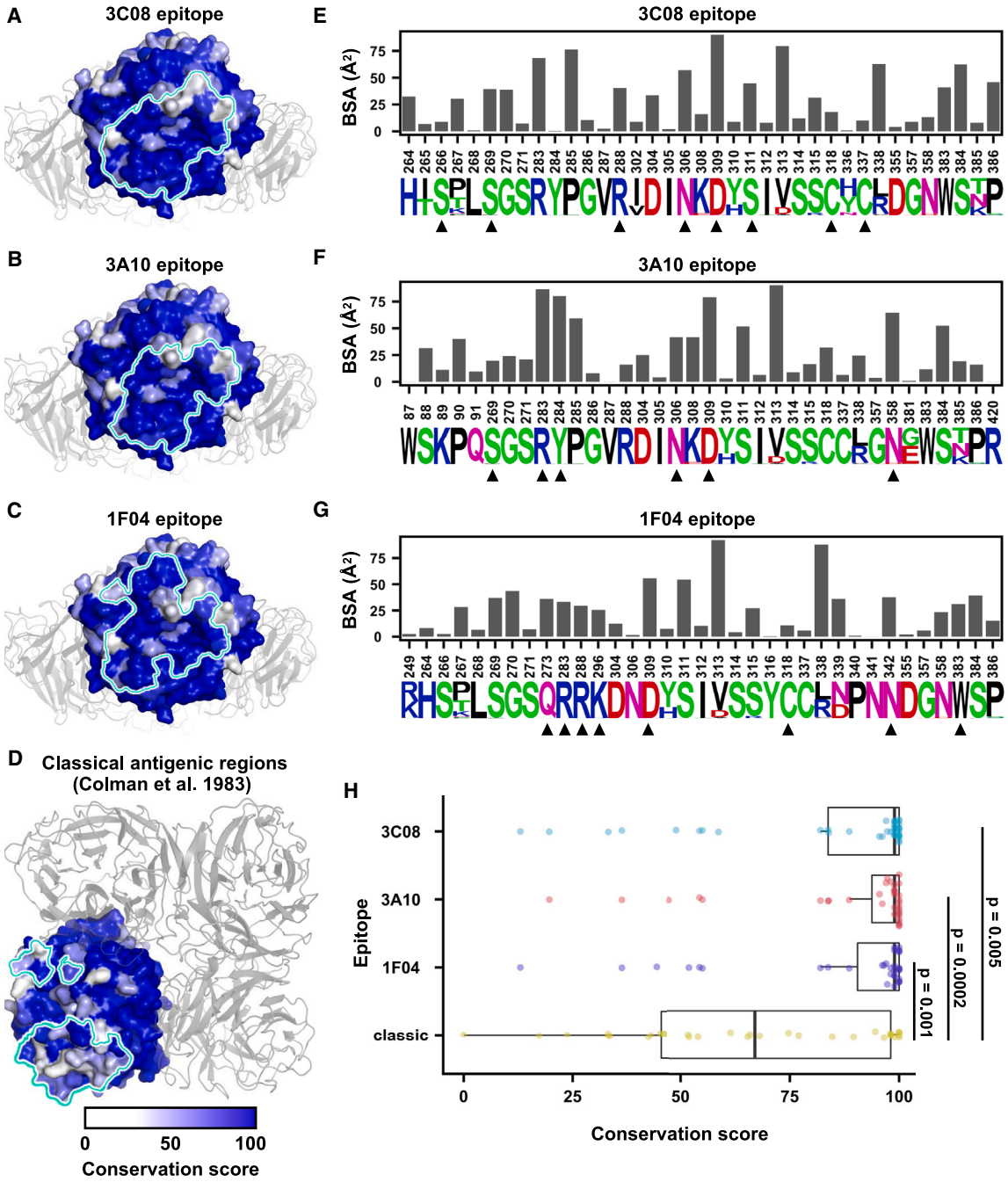

Figure 3. Sequence conservation of the underside epitopes

(A–D) Sequence conservation score for each residue is shown on the NA structure (PDB: 7U4F).[32] A high conservation score indicates high sequence conservation. The epitopes of (A) 3C08, (B) 3A10, (C) 1F04, and (D), the classical antigenic regions,[12] are indicated by the cyan outline.

(E–G) The bar charts indicate the buried surface area (BSA) of each residue in the epitopes of (E) 3C08, (F) 3A10, and (G) 1F04 upon binding. The sequence logos represent the sequence diversity of each epitope residue in natural human H3N2 strains from 1968 to 2020. Residues with side chains that H-bond with the indicated antibody are labeled by a black triangle underneath the sequence logo.

(H) Sequence conservation scores of individual residues in the antibody epitopes as well as the classical antigenic regions[12] are compared. The distributions of sequence conservation scores are shown as boxplots. p values are calculated by two-sided Wilcoxon rank-sum test.

See also Table S4.

However, Bei89 NA, which had D358, showed no detectable binding to 1F04, whereas SD93 NA, which had N358, showed strong binding activity to 1F04 (K_D = 10 nM) (Table 1; Figure S3). Together, our structural analysis implies that the binding activity of antibodies to the underside of NA head domain can be influenced by natural amino acid variants outside of the epitope.

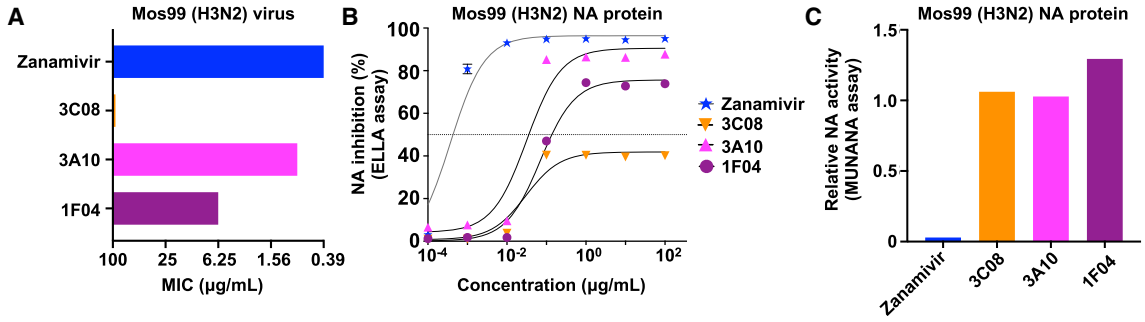

Figure 4. *In vitro* functional activity of the three antibodies

(A) Virus growth inhibition assay against recombinant viruses that carried NA from Mos99 (H3N2). The other seven segments of the recombinant viruses were from A/Puerto Rico/8/1934 (PR8). Zanamivir is used as a positive control. Minimum inhibitory concentration (MIC) is shown.

(B) NA inhibition activity of 3C08, 3A10, and 1F04 was measured by ELLA assays, using recombinant Mos99 NA protein.

(C) NA inhibition activity of 3C08, 3A10, and 1F04 at 100 μg/mL, and zanamivir (positive control) at 100 ng/mL was tested by MUNANA assays using Mos99 NA protein. Relative NA activity was computed by normalizing the NA activity to a negative control with no antibody.

3C08, 1F04, and 3A10 have different viral growth inhibition activity *in vitro*

Although 3C08, 3A10, and 1F04 had highly overlapping epitopes, they exerted very different levels of viral growth inhibition (Figure 4A). 3A10 and 1F04 inhibited the growth of A/Puerto Rico/8/1934 (PR8) carrying Mos99 NA (7:1 reassortant virus) with minimum inhibitory concentration (MIC) values of 0.78 and 6.25 μg/mL, respectively. In contrast, 3C08 exhibited no viral growth inhibition activity in this assay. We further measured the ability of 3C08, 3A10, and 1F04 in inhibiting Mos99 NA activity using an enzyme-linked lectin assay (ELLA) (Figure 4B). Consistent with the results from the viral growth inhibition assay, 3A10 had the strongest NA inhibition activity in the ELLA with a 50% inhibitory concentration (IC_{50}) value of 0.03 μg/mL, followed by 1F04 (IC_{50} = 0.07 μg/mL) and 3C08 (IC_{50} > 100 μg/mL). Nonetheless, 3C08 did show a detectable level of NA inhibition activity in the ELLA, albeit below 50%.

Because the NA active site did not overlap with the epitopes of 3C08, 3A10, and 1F04, we hypothesized that the NA inhibition activity of 3C08, 3A10, and 1F04 in the ELLA was mainly attributed to steric hindrance of substrate binding. ELLA employs fetuin, which is a highly glycosylated serum protein, as substrate for NA. Another method for measuring NA activity is to use 2′-(4-methylumbelliferyl)-α-d-N-acetylneuraminic acid (MUNANA), which is a small molecule substrate for NA. If NA inhibition activity of an antibody in the ELLA was conferred by steric hindrance, it would not inhibit the NA enzymatic activity on a small molecule substrate. Indeed, none of 3C08, 3A10, and 1F04 could inhibit the NA activity when MUNANA was used as substrate (Figure 4C), substantiating our hypothesis. Because steric hindrance was a determinant for the NA inhibition activity of these antibodies, their angles of approach for binding were likely functionally relevant. Consistently, 3A10, 3C08, and 1F04, which had very different angles of approach to NA, had different NA inhibition activity and viral growth inhibition activity yet similar binding activity against Mos99.

NA antibodies confer protection *in vivo* with unique dependencies on Fc effector function

The *in vivo* protection activity of 3C08, 3A10, and 1F04 was tested. All three antibodies showed prophylactic protection *in vivo* at 5 mg/kg against a lethal challenge of PR8 with Mos99 NA (7:1 reassortant virus) (Figure S7), based on the weight loss profiles (Figure 5A), survival analysis (Figure 5B), and lung viral titer at day 3 post-infection (Figure 5C). We also tested their prophylactic protection *in vivo* against PR8 with Mos99 NA at lower antibody doses, namely, 1 and 0.3 mg/kg (Figures 5D, 5E, 5G, and 5H). Although all mice that were prophylactic treated with 1 mg/kg of 3A10 or 1F04 survived, only 40% mice (2/5) with 1 mg/kg of 3C08 survived (Figure 5G). In addition, none of the mice that were prophylactic treated with 0.3 mg/kg of 3C08 survived, whereas the survival rates of mice with 0.3 mg/kg of 3A10 and 1F04 were 60% (3/5) and 20% (1/5), respectively (Figure 5H). These results indicated that the *in vivo* protection activity of 3C08, 3A10, and 1F04 antibodies correlated with their viral growth inhibition activity *in vitro*, in which 3A10 was the strongest and 3C08 was the weakest (Figure 4A).

We further showed that all three NA antibodies could confer therapeutic protection *in vivo* against PR8 with Mos99 NA (Figures 5F and 5I) as well as prophylactic protection *in vivo* against PR8 with an NA from a more recent H3N2 strain, A/Singapore/INFIMH-16-0019/2016 (Sing16) (Figures 5J and 5K). Because 3C08 had minimal viral growth inhibition activity *in vitro* but could confer *in vivo* protection (Figure 4A), our data suggested that Fc effector functions were critical for its *in vivo* protection activity. Consistently, 3C08, 3A10, and 1F04 could all elicit antibody-dependent cell-mediated cytotoxicity (ADCC) reporter assay activity *in vitro* (Figures 6A and 6B).

To examine the importance of Fc effector functions, we created a LALA-PG variant for each of the three antibodies to eliminate their Fc effector functions.[35] Although LALA-PG variants of all three antibodies could confer prophylactic protection *in vivo* (Figures 6C and 6D), mice treated with 3C08 LALA-PG had significantly more weight loss than those with 3C08 wild type (WT) from day 3 post-infection onward (p values < 0.05, two-tailed Student's t test, Figures 5A, 6C, and 6F). Consistently, the lung viral titer at day 3 post-infection was around one log higher in mice treated with 3C08 LALA-PG than those with 3C08 WT (p value = 0.015,

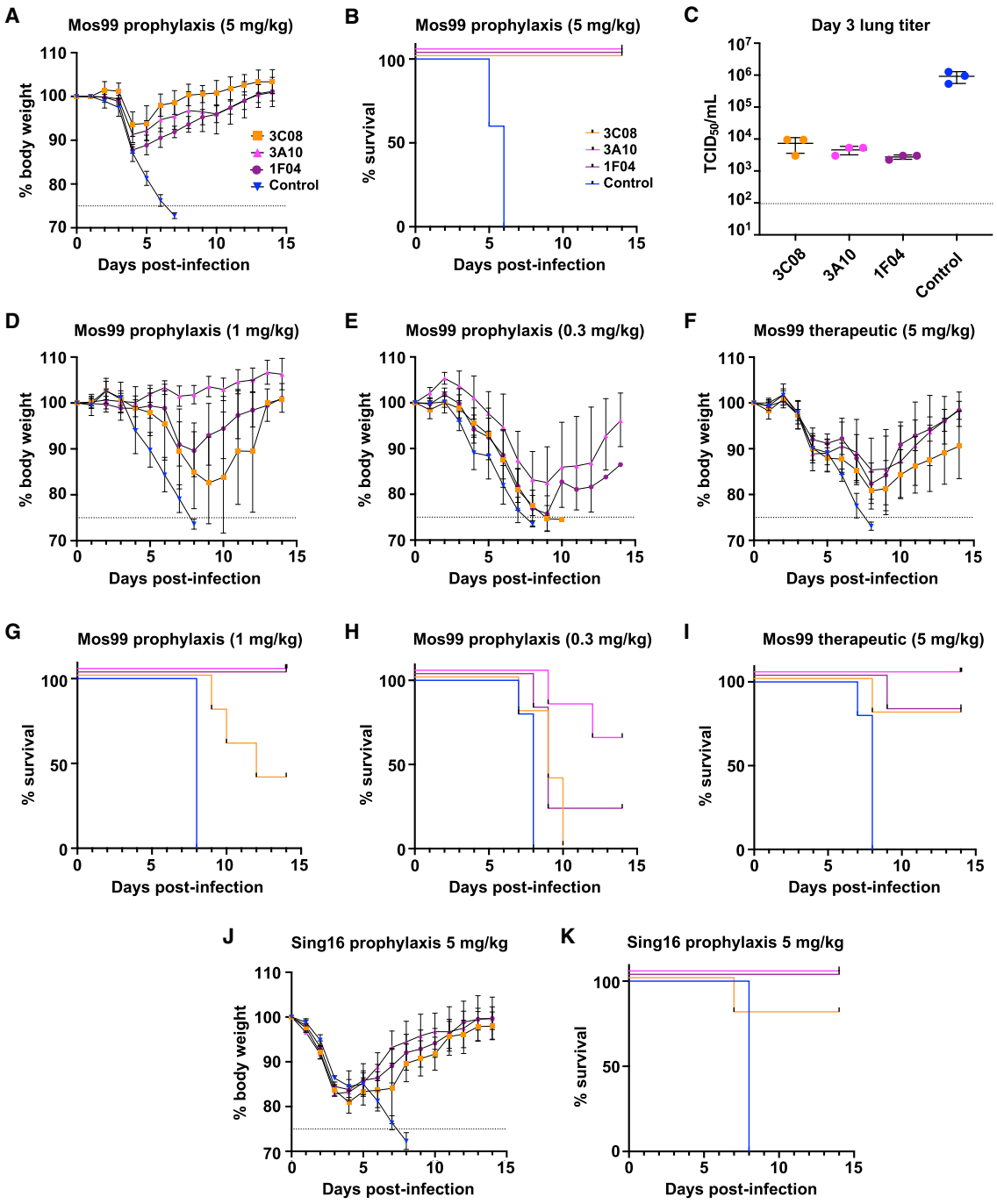

Figure 5. *In vivo* protection activity of the three antibodies

(A–C) Female BALB/c mice at 6 weeks old were injected intraperitoneally with 5 mg/kg of the indicated antibody 2 h prior to challenge with 5 LD_{50} of a recombinant virus that carried NA from H3N2 Mos99 with the other 7 segments from A/Puerto Rico/8/1934 (PR8). A representative experiment from two independent replicates with similar results is shown.

(A) The mean percentage of body weight change post-infection is shown (n = 5). The humane endpoint, which was defined as a weight loss of 25% from initial weight on day 0, is shown as a dotted line.

(B) Kaplan-Meier survival curves are shown (n = 5).

(C) Lung viral titers on day 3 after infection are shown (n = 3). Solid black lines indicate mean ± SD. The dotted line represents the lower detection limit.

(D–I) Same as (A) and (B), except (D) and (G) 1 mg/kg of the indicated antibody was injected intraperitoneally 2 h prior to challenge, (E and H) 0.3 mg/kg of the indicated antibody was injected intraperitoneally 2 h prior to challenge, and (F and I) 5 mg/kg of the indicated antibody was injected intraperitoneally 72 h after challenge.

(legend continued on next page)

two-tailed Student's t test, Figures 5C, 6E, and 6G). In contrast, such differences were much less apparent, albeit statistically significant, for 1F04, and insignificant for 3A10. Therefore, the importance of Fc effector functions in protection activity *in vivo* seemed to inversely correlate with viral growth inhibition activity *in vitro* (Figure 4E).

DISCUSSION

Although it has been known for decades that NA antibodies are protective,[36,37] NA immunity gained little attention until mid-2010s.[8,9,38] The classical antigenic regions of NA all reside in the upper face of the head domain.[12] However, more recent structural studies of NA antibodies demonstrate that the lateral face of NA head domain can also be targeted by antibodies,[14,16,20] which align with the results from escape selection experiments.[39,40] Together with our identification of antibodies recognizing the underside of NA head domain, it seems like most surface of NA head domain can be targeted by antibodies. Nevertheless, we acknowledge that these NA antibodies with structural information available are from different sources—most are from infected patients[16–19] or immunized mice,[13–15,41–46] whereas 3C08, 3A10, and 1F04 in this study are from a vaccinated individual. As we learn more about antibody epitopes on NA, future studies should explore the immunodominance hierarchy of these epitopes, which will provide important insights into NA antigenic drift and next-generation vaccine design.

A major highlight of this study is that human antibodies to the underside of NA head domain have diverse germline gene usages. Therefore, these types of antibodies may be relatively common, although its exact prevalence in the human population remains to be explored. In fact, a previous study has identified another N2 antibody from human, NDS.1, that purportedly targets the underside of NA head domain.[47] However, NDS.1 was only characterized by low-resolution negative-stain EM analysis, which prevents its epitope to be precisely defined. Antibody escape mutations in N1 NA further suggest that human antibodies can target the underside of NA head domain in other influenza subtypes,[39] although their structural mechanisms remain to be explored. It is intriguing to see that antibody to the underside of NA head domain, which is far from the active site, can have reasonable viral growth inhibition activity and NA inhibition activity in ELLA, as exemplified by 3A10 and 1F04. Similar observations have been made for antibodies to other NA epitopes that are distal from the active site.[14,16,20,22] As a result, sterically hindering NA to access its natural substrates is a shared mechanism among antibodies to diverse epitopes on NA.

Another interesting observation in this study is that although the NA inhibition activity of 3C08 plateaus at 40% in ELLA, it can confer *in vivo* protection even without the Fc effector functions. This indicates that partial NA inhibition is sufficient to provide Fc-independent protection *in vivo*. In contrast, 3C08 has no detectable viral growth inhibition activity *in vitro*, showing the limitation of using *in vitro* viral growth inhibition assay to assess NA antibody activity. Given that ELLA is the standard assay for measuring NA antibody titer,[48] it will be important to understand the relationship between NA inhibition activity in ELLA and *in vivo* protective activity.

Identification of conserved epitopes is key to developing a more broadly protective vaccine.[49] For example, the CD4 binding site of human immunodeficiency virus type 1 (HIV-1) envelope glycoprotein was structurally defined as a neutralizing epitope in 2007.[50] This finding facilitates the development of an HIV-1 vaccine candidate against the CD4 binding site,[51,52] which has performed well in a phase 1 clinical trial (NCT03547245).[53] As for influenza virus, the highly conserved HA stem was structurally defined as a neutralizing epitope in 2009.[54] Subsequently, the HA stem became the major target for the development of universal influenza vaccine candidates,[55–57] which have shown promising results in two phase 1 clinical trials (NCT03300050 and NCT03814720).[58,59] Similarly, future immunogen design studies should explore whether NA antibody response can be focused on cross-protective epitopes. Ultimately, we may be able to develop a broadly protective vaccine that can induce cross-protective polyclonal response to multiple conserved epitopes on both HA and NA.

Limitations of the study

Although 3C08, 3A10, and 1F04 were isolated from the plasmablasts after vaccination, we cannot confidently conclude whether they represented memory B cell response or *de novo* B cell activation. This could potentially be addressed by examining the memory B cell repertoire before vaccination. However, such samples were not available for this study. Nevertheless, the number of SHMs in the heavy-chain V genes of 3C08, 3A10, and 1F04 (7.2%, 10.1%, and 7.5% at the nucleotide level, respectively) was not low,[60] suggesting that these antibodies were from memory B cell responses. Another limitation of the study is the insufficient structural information to investigate how non-epitope amino acid variants in NA could affect the binding affinity of these NA antibodies. We postulate that non-epitope amino acid variants can influence antibody binding by modulating the backbone conformation of NA. Consistently, our previous study has shown the backbone conformation of NA has changed during the natural evolution of human H3N2 virus.[32] However, structural information of NA is only available for a few human H3N2 strains, which prevented us from performing detailed structural analysis of non-epitope amino acid variants.

STAR★METHODS

Detailed methods are provided in the online version of this paper and include the following:

(J and K) Same as (A) and (B), except a recombinant virus that carried NA from H3N2 A/Singapore/INFIMH-16-0019/2016 (Sing16) with the other seven segments from A/Puerto Rico/8/1934 (PR8) was used. 2B04, which is a severe acute respiratory syndrome coronavirus 2 (SARS-CoV-2) spike antibody,[33] was used as a control.
See also Figure S7.

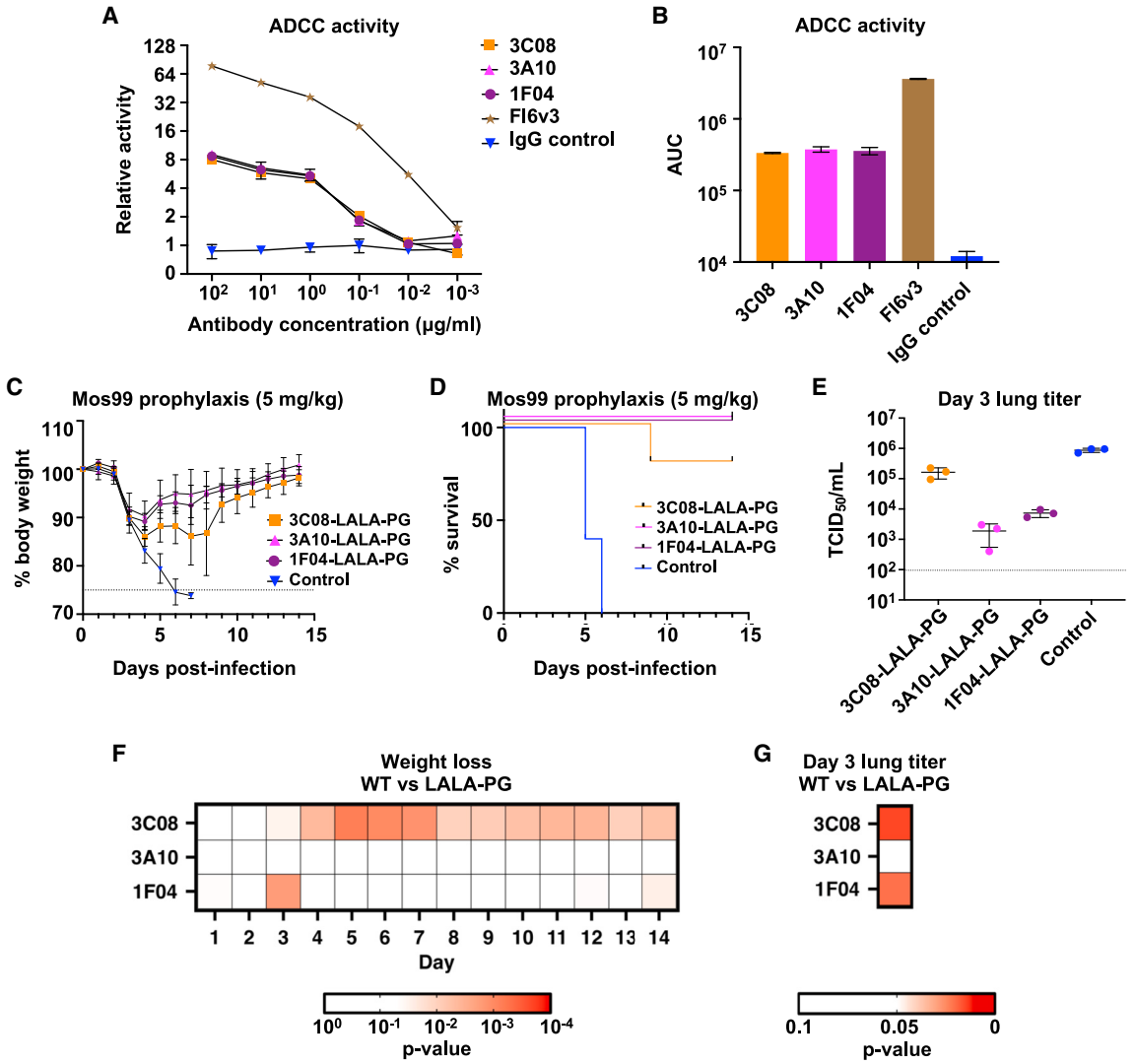

Figure 6. Fc effector functions contribute to *in vivo* protection

(A and B) Antibody-dependent cellular cytotoxicity (ADCC) activity of the three antibodies was measured. FI6v3, which is an antibody to hemagglutinin (HA) and has known ADCC reporter assay activity against H3N2,[34] was used as a positive control. IgG from human serum (Sigma, catalog #: I4506-50MG) was used as a negative control. (A) Titration curve and (B) area under the curve (AUC) are shown.

(C–E) Same as Figures 5A–5C, except antibodies with LALA-PG mutations, which eliminate Fc effector functions,[35] were used.

(F) p value of the difference in weight loss between mice treated with the indicated antibody and its corresponding LALA-PG mutant at each day post-infection is computed by two-tailed Student's t test.

(G) p value of the difference in lung viral titer at day 3 post-infection between mice treated with the indicated antibody and its corresponding LALA-PG mutant is computed by two-tailed Student's t test.

See also Figure S7.

- Sequence conservation analysis
- Enzyme-linked lectin assay (ELLA)
- MUNANA assay
- Virus growth inhibition assay
- ADCC reporter bioassay
- Prophylactic and therapeutic protection experiments

- QUANTIFICATION AND STATISTICAL ANALYSIS

SUPPLEMENTAL INFORMATION

Supplemental information can be found online at https://doi.org/10.1016/j.immuni.2023.10.005.

ACKNOWLEDGMENTS

We are grateful to the cryo-EM Core and the Core Facility for Advanced Research Computing at Case Western Reserve University for access of cryo-EM instrumentation and data-processing resources, respectively. This work was supported by the Basic Science Research Program through the National Research Foundation of Korea (NRF) funded by the Ministry of Education 2021R1A6A3A03041509 (W.K.), the Calmette and Yersin scholarship from the Pasteur International Network Association (H.L.), the Emergency Key Program of Guangzhou Laboratory (grant no. EKPG22-30-6) (C.K.P.M.), the visiting scientist scheme from Lee Kong Chian School of Medicine, Nanyang Technological University, Singapore (C.K.P.M.), National Institutes of Health (NIH) R01 AI165475 (N.C.W.), DP2 AT011966 (N.C.W.), U01 AI141990 (A.H.E.), U01 AI150747 (A.H.E.), U01 AI144616 (A.H.E.), the Michelson Prizes for Human Immunology and Vaccine Research (N.C.W.), and the Searle Scholars Program (N.C.W.). This study was also partially supported by the NIAID Centers of Excellence for Influenza Research and Response contract 75N93021C00014 (F.K.) and by the NIAID Collaborative Influenza Vaccine Innovation Centers (CIVICs) contract 75N93019C00051 (F.K.).

AUTHOR CONTRIBUTIONS

R.L., W.K., H.L., Z.M., M.J.S., C.K.P.M., F.K., X.D., A.H.E., and N.C.W. conceived and designed the study. W.K., A.J.S., J.S.T., R.M.P., and A.H.E. isolated the antibodies. R.L., Z.M., X.D., and N.C.W. performed structural analysis of the antibodies. R.L., W.K., H.L., M.J.S., A.J.S., J.S.T., T.J.C.T., Y.W., W.O.O., W.L., J.R.-C., C.T., C.S.G., C.B.B., C.K.P.M., and F.K. performed functional characterization of the antibodies. R.L., W.K., H.L., and N.C.W. wrote the paper and all authors reviewed and edited the paper.

DECLARATION OF INTERESTS

N.C.W. consults for HeliXon. The Ellebedy laboratory received funding under sponsored research agreements from Moderna, Emergent BioSolutions, and AbbVie that are unrelated to the data presented in this study. A.H.E. is a consultant for Mubadala Investment Company and the founder of ImmuneBio Consulting. A.J.S., J.S.T., and A.H.E. are recipients of a licensing agreement with AbbVie that is unrelated to the data presented in this study. The Icahn School of Medicine at Mount Sinai has filed patent application on influenza virus vaccines that name F.K. as inventor. In addition, F.K. is currently consulting for Pfizer, Third Rock Ventures, and Avimex and has received support for vaccine research and development by Pfizer, GSK, and Dynavax.

Received: November 1, 2022
Revised: July 19, 2023
Accepted: October 10, 2023
Published: November 14, 2023

REFERENCES

1. Koutsakos, M., Wheatley, A.K., Laurie, K., Kent, S.J., and Rockman, S. (2021). Influenza lineage extinction during the COVID-19 pandemic? Nat. Rev. Microbiol. *19*, 741–742. https://doi.org/10.1038/s41579-021-00642-4.

2. Merced-Morales, A., Daly, P., Abd Elal, A.I., Ajayi, N., Annan, E., Budd, A., Barnes, J., Colon, A., Cummings, C.N., Iuliano, A.D., et al. (2022). Influenza activity and composition of the 2022–23 influenza vaccine - United States, 2021–22 season. MMWR Morb. Mortal. Wkly. Rep. *71*, 913–919. https://doi.org/10.15585/mmwr.mm7129a1.

3. Monto, A.S., Petrie, J.G., Cross, R.T., Johnson, E., Liu, M., Zhong, W., Levine, M., Katz, J.M., and Ohmit, S.E. (2015). Antibody to influenza virus neuraminidase: an independent correlate of protection. J. Infect. Dis. *212*, 1191–1199. https://doi.org/10.1093/infdis/jiv195.

4. Couch, R.B., Atmar, R.L., Franco, L.M., Quarles, J.M., Wells, J., Arden, N., Niño, D., and Belmont, J.W. (2013). Antibody correlates and predictors of immunity to naturally occurring influenza in humans and the importance of antibody to the neuraminidase. J. Infect. Dis. *207*, 974–981. https://doi.org/10.1093/infdis/jis935.

5. Memoli, M.J., Shaw, P.A., Han, A., Czajkowski, L., Reed, S., Athota, R., Bristol, T., Fargis, S., Risos, K., Powers, J.H., et al. (2016). Evaluation of antihemagglutinin and antineuraminidase antibodies as correlates of protection in an influenza A/H1N1 virus healthy human challenge model. mBio *7*. e00417–e00416. https://doi.org/10.1128/mBio.00417-16.

6. Weiss, C.D., Wang, W., Lu, Y., Billings, M., Eick-Cost, A., Couzens, L., Sanchez, J.L., Hawksworth, A.W., Seguin, P., Myers, C.A., et al. (2020). Neutralizing and neuraminidase antibodies correlate with protection against influenza during a late season A/H3N2 outbreak among unvaccinated military recruits. Clin. Infect. Dis. *71*, 3096–3102. https://doi.org/10.1093/cid/ciz1198.

7. Maier, H.E., Nachbagauer, R., Kuan, G., Ng, S., Lopez, R., Sanchez, N., Stadlbauer, D., Gresh, L., Schiller, A., Rajabhathor, A., et al. (2020). Pre-existing antineuraminidase antibodies are associated with shortened duration of influenza A(H1N1)pdm virus shedding and illness in naturally infected adults. Clin. Infect. Dis. *70*, 2290–2297. https://doi.org/10.1093/cid/ciz639.

8. Krammer, F., Fouchier, R.A.M., Eichelberger, M.C., Webby, R.J., Shaw-Saliba, K., Wan, H., Wilson, P.C., Compans, R.W., Skountzou, I., and Monto, A.S. (2018). NAction! How can neuraminidase-based immunity contribute to better influenza virus vaccines? mBio *9*, e02332-17. https://doi.org/10.1128/mBio.02332-17.

9. Eichelberger, M.C., and Monto, A.S. (2019). Neuraminidase, the forgotten surface antigen, emerges as an influenza vaccine target for broadened protection. J. Infect. Dis. *219* (*Suppl 1*), S75–S80. https://doi.org/10.1093/infdis/jiz017.

10. McAuley, J.L., Gilbertson, B.P., Trifkovic, S., Brown, L.E., and McKimm-Breschkin, J.L. (2019). Influenza virus neuraminidase structure and functions. Front. Microbiol. *10*, 39. https://doi.org/10.3389/fmicb.2019.00039.

11. Varghese, J.N., Laver, W.G., and Colman, P.M. (1983). Structure of the influenza virus glycoprotein antigen neuraminidase at 2.9 A resolution. Nature *303*, 35–40. https://doi.org/10.1038/303035a0.

12. Colman, P.M., Varghese, J.N., and Laver, W.G. (1983). Structure of the catalytic and antigenic sites in influenza virus neuraminidase. Nature *303*, 41–44. https://doi.org/10.1038/303041a0.

13. Venkatramani, L., Bochkareva, E., Lee, J.T., Gulati, U., Graeme Laver, W., Bochkarev, A., and Air, G.M. (2006). An epidemiologically significant epitope of a 1998 human influenza virus neuraminidase forms a highly hydrated interface in the NA-antibody complex. J. Mol. Biol. *356*, 651–663. https://doi.org/10.1016/j.jmb.2005.11.061.

14. Wan, H., Yang, H., Shore, D.A., Garten, R.J., Couzens, L., Gao, J., Jiang, L., Carney, P.J., Villanueva, J., Stevens, J., et al. (2015). Structural characterization of a protective epitope spanning A(H1N1)pdm09 influenza virus neuraminidase monomers. Nat. Commun. *6*, 6114. https://doi.org/10.1038/ncomms7114.

15. Wan, H., Gao, J., Yang, H., Yang, S., Harvey, R., Chen, Y.Q., Zheng, N.Y., Chang, J., Carney, P.J., Li, X., et al. (2019). The neuraminidase of A(H3N2) influenza viruses circulating since 2016 is antigenically distinct from the A/Hong Kong/4801/2014 vaccine strain. Nat. Microbiol. *4*, 2216–2225. https://doi.org/10.1038/s41564-019-0522-6.

16. Zhu, X., Turner, H.L., Lang, S., McBride, R., Bangaru, S., Gilchuk, I.M., Yu, W., Paulson, J.C., Crowe, J.E., Jr., Ward, A.B., et al. (2019). Structural basis of protection against H7N9 influenza virus by human anti-N9 neuraminidase antibodies. Cell Host Microbe *26*, 729–738.e4. https://doi.org/10.1016/j.chom.2019.10.002.

17. Stadlbauer, D., Zhu, X., McMahon, M., Turner, J.S., Wohlbold, T.J., Schmitz, A.J., Strohmeier, S., Yu, W., Nachbagauer, R., Mudd, P.A., et al. (2019). Broadly protective human antibodies that target the active site of influenza virus neuraminidase. Science *366*, 499–504. https://doi.org/10.1126/science.aay0678.

18. Jiang, H., Peng, W., Qi, J., Chai, Y., Song, H., Bi, Y., Rijal, P., Wang, H., Oladejo, B.O., Liu, J., et al. (2020). Structure-based modification of an anti-neuraminidase human antibody restores protection efficacy against the drifted influenza virus. mBio *11*, e02315-20. https://doi.org/10.1128/mBio.02315-20.

19. Madsen, A., Dai, Y.N., McMahon, M., Schmitz, A.J., Turner, J.S., Tan, J., Lei, T., Alsoussi, W.B., Strohmeier, S., Amor, M., et al. (2020). Human antibodies targeting influenza B virus neuraminidase active site are broadly protective. Immunity *53*, 852–863.e7. https://doi.org/10.1016/j.immuni.2020.08.015.

20. Wohlbold, T.J., Podolsky, K.A., Chromikova, V., Kirkpatrick, E., Falconieri, V., Meade, P., Amanat, F., Tan, J., tenOever, B.R., Tan, G.S., et al. (2017). Broadly protective murine monoclonal antibodies against influenza B virus target highly conserved neuraminidase epitopes. Nat. Microbiol. *2*, 1415–1424. https://doi.org/10.1038/s41564-017-0011-8.

21. Momont, C., Dang, H.V., Zatta, F., Hauser, K., Wang, C., di Iulio, J., Minola, A., Czudnochowski, N., De Marco, A., Branch, K., et al. (2023). A pan-influenza antibody inhibiting neuraminidase via receptor mimicry. Nature *618*, 590–597. https://doi.org/10.1038/s41586-023-06136-y.

22. Gilchuk, I.M., Bangaru, S., Gilchuk, P., Irving, R.P., Kose, N., Bombardi, R.G., Thornburg, N.J., Creech, C.B., Edwards, K.M., Li, S., et al. (2019). Influenza H7N9 virus neuraminidase-specific human monoclonal antibodies inhibit viral egress and protect from lethal influenza infection in mice. Cell Host Microbe *26*, 715–728.e8. https://doi.org/10.1016/j.chom.2019.10.003.

23. Erbelding, E.J., Post, D.J., Stemmy, E.J., Roberts, P.C., Augustine, A.D., Ferguson, S., Paules, C.I., Graham, B.S., and Fauci, A.S. (2018). A universal influenza vaccine: the strategic plan for the National Institute of Allergy and Infectious Diseases. J. Infect. Dis. *218*, 347–354. https://doi.org/10.1093/infdis/jiy103.

24. Turner, J.S., Zhou, J.Q., Han, J., Schmitz, A.J., Rizk, A.A., Alsoussi, W.B., Lei, T., Amor, M., McIntire, K.M., Meade, P., et al. (2020). Human germinal centres engage memory and naive B cells after influenza vaccination. Nature *586*, 127–132. https://doi.org/10.1038/s41586-020-2711-0.

25. Wang, F., Wan, Z., Wu, J., Wang, Y., Fu, H., Shao, H., Qian, K., Gao, W., Ye, J., and Qin, A. (2021). A cross-reactive monoclonal antibody against neuraminidases of both H9N2 and H3N2 influenza viruses shows protection in mice challenging models. Front. Microbiol. *12*, 730449. https://doi.org/10.3389/fmicb.2021.730449.

26. Gulati, U., Hwang, C.C., Venkatramani, L., Gulati, S., Stray, S.J., Lee, J.T., Laver, W.G., Bochkarev, A., Zlotnick, A., and Air, G.M. (2002). Antibody epitopes on the neuraminidase of a recent H3N2 influenza virus (A/Memphis/31/98). J. Virol. *76*, 12274–12280.

27. DeDiego, M.L., Chiem, K., and Topham, D.J. (2018). Directed selection of amino acid changes in the influenza hemagglutinin and neuraminidase affecting protein antigenicity. Vaccine *36*, 6383–6392. https://doi.org/10.1016/j.vaccine.2018.09.005.

28. Kirkpatrick Roubidoux, E., McMahon, M., Carreño, J.M., Capuano, C., Jiang, K., Simon, V., van Bakel, H., Wilson, P., and Krammer, F. (2021). Identification and characterization of novel antibody epitopes on the N2 neuraminidase. mSphere *6*, e00958-20. https://doi.org/10.1128/mSphere.00958-20.

29. Wan, Z., Ye, J., Sang, J., Shao, H., Qian, K., Jin, W., Qin, A., and Wan, H. (2016). Identification of amino acids in H9N2 influenza virus neuraminidase that are critical for the binding of two mouse monoclonal antibodies. Vet. Microbiol. *187*, 58–63. https://doi.org/10.1016/j.vetmic.2016.03.011.

30. Chen, Y.Q., Wohlbold, T.J., Zheng, N.Y., Huang, M., Huang, Y., Neu, K.E., Lee, J., Wan, H., Rojas, K.T., Kirkpatrick, E., et al. (2018). Influenza infection in humans induces broadly cross-reactive and protective neuraminidase-reactive antibodies. Cell *173*, 417–429.e10. https://doi.org/10.1016/j.cell.2018.03.030.

31. Doyle, T.M., Hashem, A.M., Li, C., Van Domselaar, G., Larocque, L., Wang, J., Smith, D., Cyr, T., Farnsworth, A., He, R., et al. (2013). Universal anti-neuraminidase antibody inhibiting all influenza A subtypes. Antiviral Res. *100*, 567–574. https://doi.org/10.1016/j.antiviral.2013.09.018.

32. Lei, R., Tan, T.J.C., Hernandez Garcia, A., Wang, Y., Diefenbacher, M., Teo, C., Gopan, G., Tavakoli Dargani, Z., Teo, Q.W., Graham, C.S., et al. (2022). Prevalence and mechanisms of evolutionary contingency in human influenza H3N2 neuraminidase. Nat. Commun. *13*, 6443. https://doi.org/10.1038/s41467-022-34060-8.

33. Alsoussi, W.B., Turner, J.S., Case, J.B., Zhao, H., Schmitz, A.J., Zhou, J.Q., Chen, R.E., Lei, T., Rizk, A.A., McIntire, K.M., et al. (2020). A potently neutralizing antibody protects mice against SARS-CoV-2 infection. J. Immunol. *205*, 915–922. https://doi.org/10.4049/jimmunol.2000583.

34. DiLillo, D.J., Tan, G.S., Palese, P., and Ravetch, J.V. (2014). Broadly neutralizing hemagglutinin stalk-specific antibodies require FcγR interactions for protection against influenza virus in vivo. Nat. Med. *20*, 143–151. https://doi.org/10.1038/nm.3443.

35. Lo, M., Kim, H.S., Tong, R.K., Bainbridge, T.W., Vernes, J.M., Zhang, Y., Lin, Y.L., Chung, S., Dennis, M.S., Zuchero, Y.J., et al. (2017). Effector-attenuating substitutions that maintain antibody stability and reduce toxicity in mice. J. Biol. Chem. *292*, 3900–3908. https://doi.org/10.1074/jbc.M116.767749.

36. Couch, R.B., Kasel, J.A., Gerin, J.L., Schulman, J.L., and Kilbourne, E.D. (1974). Induction of partial immunity to influenza by a neuraminidase-specific vaccine. J. Infect. Dis. *129*, 411–420. https://doi.org/10.1093/infdis/129.4.411.

37. Murphy, B.R., Kasel, J.A., and Chanock, R.M. (1972). Association of serum anti-neuraminidase antibody with resistance to influenza in man. N. Engl. J. Med. *286*, 1329–1332. https://doi.org/10.1056/NEJM197206222862502.

38. Eichelberger, M.C., and Wan, H. (2015). Influenza neuraminidase as a vaccine antigen. Curr. Top. Microbiol. Immunol. *386*, 275–299. https://doi.org/10.1007/82_2014_398.

39. Kirkpatrick Roubidoux, E., Sano, K., McMahon, M., Carreño, J.M., Capuano, C., Jiang, K., Simon, V., van Bakel, H., Wilson, P., and Krammer, F. (2022). Novel epitopes of the influenza virus N1 neuraminidase targeted by human monoclonal antibodies. J. Virol. *96*, e0033222. https://doi.org/10.1128/jvi.00332-22.

40. Wan, H., Gao, J., Xu, K., Chen, H., Couzens, L.K., Rivers, K.H., Easterbrook, J.D., Yang, K., Zhong, L., Rajabi, M., et al. (2013). Molecular basis for broad neuraminidase immunity: conserved epitopes in seasonal and pandemic H1N1 as well as H5N1 influenza viruses. J. Virol. *87*, 9290–9300. https://doi.org/10.1128/JVI.01203-13.

41. Tulip, W.R., Varghese, J.N., Laver, W.G., Webster, R.G., and Colman, P.M. (1992). Refined crystal structure of the influenza virus N9 neuraminidase-NC41 Fab complex. J. Mol. Biol. *227*, 122–148. https://doi.org/10.1016/0022-2836(92)90687-f.

42. Tulip, W.R., Harley, V.R., Webster, R.G., and Novotny, J. (1994). N9 neuraminidase complexes with antibodies NC41 and NC10: empirical free energy calculations capture specificity trends observed with mutant binding data. Biochemistry *33*, 7986–7997. https://doi.org/10.1021/bi00192a002.

43. Tulip, W.R., Varghese, J.N., Webster, R.G., Laver, W.G., and Colman, P.M. (1992). Crystal structures of two mutant neuraminidase-antibody complexes with amino acid substitutions in the interface. J. Mol. Biol. *227*, 149–159. https://doi.org/10.1016/0022-2836(92)90688-g.

44. Malby, R.L., Tulip, W.R., Harley, V.R., McKimm-Breschkin, J.L., Laver, W.G., Webster, R.G., and Colman, P.M. (1994). The structure of a complex between the NC10 antibody and influenza virus neuraminidase and comparison with the overlapping binding site of the NC41 antibody. Structure *2*, 733–746.

45. Malby, R.L., McCoy, A.J., Kortt, A.A., Hudson, P.J., and Colman, P.M. (1998). Three-dimensional structures of single-chain Fv-neuraminidase complexes. J. Mol. Biol. *279*, 901–910. https://doi.org/10.1006/jmbi.1998.1794.

46. Webster, R.G., Air, G.M., Metzger, D.W., Colman, P.M., Varghese, J.N., Baker, A.T., and Laver, W.G. (1987). Antigenic structure and variation in an influenza virus N9 neuraminidase. J. Virol. *61*, 2910–2916.

47. Casalino, L., Seitz, C., Lederhofer, J., Tsybovsky, Y., Wilson, I.A., Kanekiyo, M., and Amaro, R.E. (2022). Breathing and tilting: mesoscale simulations illuminate influenza glycoprotein vulnerabilities. ACS Cent. Sci. *8*, 1646–1663. https://doi.org/10.1021/acscentsci.2c00981.

48. Eichelberger, M.C., Couzens, L., Gao, Y., Levine, M., Katz, J., Wagner, R., Thompson, C.I., Höschler, K., Laurie, K., Bai, T., et al. (2016). Comparability of neuraminidase inhibition antibody titers measured by enzyme-linked lectin assay (ELLA) for the analysis of influenza vaccine immunogenicity. Vaccine *34*, 458–465. https://doi.org/10.1016/j.vaccine.2015.12.022.

49. Caradonna, T.M., and Schmidt, A.G. (2021). Protein engineering strategies for rational immunogen design. npj Vaccines *6*, 154. https://doi.org/10.1038/s41541-021-00417-1.

50. Zhou, T., Xu, L., Dey, B., Hessell, A.J., Van Ryk, D., Xiang, S.H., Yang, X., Zhang, M.Y., Zwick, M.B., Arthos, J., et al. (2007). Structural definition of a conserved neutralization epitope on HIV-1 gp120. Nature *445*, 732–737. https://doi.org/10.1038/nature05580.

51. Jardine, J., Julien, J.P., Menis, S., Ota, T., Kalyuzhniy, O., McGuire, A., Sok, D., Huang, P.S., MacPherson, S., Jones, M., et al. (2013). Rational HIV immunogen design to target specific germline B cell receptors. Science *340*, 711–716. https://doi.org/10.1126/science.1234150.

52. Jardine, J.G., Ota, T., Sok, D., Pauthner, M., Kulp, D.W., Kalyuzhniy, O., Skog, P.D., Thinnes, T.C., Bhullar, D., Briney, B., et al. (2015). HIV-1 VACCINES. Priming a broadly neutralizing antibody response to HIV-1 using a germline-targeting immunogen. Science *349*, 156–161. https://doi.org/10.1126/science.aac5894.

53. Leggat, D.J., Cohen, K.W., Willis, J.R., Fulp, W.J., deCamp, A.C., Kalyuzhniy, O., Cottrell, C.A., Menis, S., Finak, G., Ballweber-Fleming, L., et al. (2022). Vaccination induces HIV broadly neutralizing antibody precursors in humans. Science *378*, eadd6502. https://doi.org/10.1126/science.add6502.

54. Ekiert, D.C., Bhabha, G., Elsliger, M.A., Friesen, R.H., Jongeneelen, M., Throsby, M., Goudsmit, J., and Wilson, I.A. (2009). Antibody recognition of a highly conserved influenza virus epitope. Science *324*, 246–251. https://doi.org/10.1126/science.1171491.

55. Hai, R., Krammer, F., Tan, G.S., Pica, N., Eggink, D., Maamary, J., Margine, I., Albrecht, R.A., and Palese, P. (2012). Influenza viruses expressing chimeric hemagglutinins: globular head and stalk domains derived from different subtypes. J. Virol. *86*, 5774–5781. https://doi.org/10.1128/JVI.00137-12.

56. Impagliazzo, A., Milder, F., Kuipers, H., Wagner, M.V., Zhu, X., Hoffman, R.M., van Meersbergen, R., Huizingh, J., Wanningen, P., Verspuij, J., et al. (2015). A stable trimeric influenza hemagglutinin stem as a broadly protective immunogen. Science *349*, 1301–1306. https://doi.org/10.1126/science.aac7263.

57. Yassine, H.M., Boyington, J.C., McTamney, P.M., Wei, C.J., Kanekiyo, M., Kong, W.P., Gallagher, J.R., Wang, L., Zhang, Y., Joyce, M.G., et al. (2015). Hemagglutinin-stem nanoparticles generate heterosubtypic influenza protection. Nat. Med. *21*, 1065–1070. https://doi.org/10.1038/nm.3927.

58. Nachbagauer, R., Feser, J., Naficy, A., Bernstein, D.I., Guptill, J., Walter, E.B., Berlanda-Scorza, F., Stadlbauer, D., Wilson, P.C., Aydillo, T., et al. (2021). A chimeric hemagglutinin-based universal influenza virus vaccine approach induces broad and long-lasting immunity in a randomized, placebo-controlled phase I trial. Nat. Med. *27*, 106–114. https://doi.org/10.1038/s41591-020-1118-7.

59. Widge, A.T., Hofstetter, A.R., Houser, K.V., Awan, S.F., Chen, G.L., Burgos Florez, M.C., Berkowitz, N.M., Mendoza, F., Hendel, C.S., Holman, L.A., et al. (2023). An influenza hemagglutinin stem nanoparticle vaccine induces cross-group 1 neutralizing antibodies in healthy adults. Sci. Transl. Med. *15*, eade4790. https://doi.org/10.1126/scitranslmed.ade4790.

60. Glanville, J., Kuo, T.C., von Büdingen, H.C., Guey, L., Berka, J., Sundar, P.D., Huerta, G., Mehta, G.R., Oksenberg, J.R., Hauser, S.L., et al. (2011). Naive antibody gene-segment frequencies are heritable and unaltered by chronic lymphocyte ablation. Proc. Natl. Acad. Sci. USA *108*, 20066–20071. https://doi.org/10.1073/pnas.1107498108.

61. Neumann, G., Watanabe, T., Ito, H., Watanabe, S., Goto, H., Gao, P., Hughes, M., Perez, D.R., Donis, R., Hoffmann, E., et al. (1999). Generation of influenza A viruses entirely from cloned cDNAs. Proc. Natl. Acad. Sci. USA *96*, 9345–9350.

62. Dunbar, J., Krawczyk, K., Leem, J., Marks, C., Nowak, J., Regep, C., Georges, G., Kelm, S., Popovic, B., and Deane, C.M. (2016). SAbPred: a structure-based antibody prediction server. Nucleic Acids Res. *44*, W474–W478. https://doi.org/10.1093/nar/gkw361.

63. Adams, P.D., Afonine, P.V., Bunkóczi, G., Chen, V.B., Davis, I.W., Echols, N., Headd, J.J., Hung, L.W., Kapral, G.J., Grosse-Kunstleve, R.W., et al. (2010). PHENIX: a comprehensive Python-based system for macromolecular structure solution. Acta Crystallogr. D Biol. Crystallogr. *66*, 213–221. https://doi.org/10.1107/S0907444909052925.

64. Emsley, P., Lohkamp, B., Scott, W.G., and Cowtan, K. (2010). Features and development of Coot. Acta Crystallogr. D Biol. Crystallogr. *66*, 486–501. https://doi.org/10.1107/S0907444910007493.

65. Punjani, A., Rubinstein, J.L., Fleet, D.J., and Brubaker, M.A. (2017). cryoSPARC: algorithms for rapid unsupervised cryo-EM structure determination. Nat. Methods *14*, 290–296. https://doi.org/10.1038/nmeth.4169.

66. Pettersen, E.F., Goddard, T.D., Huang, C.C., Couch, G.S., Greenblatt, D.M., Meng, E.C., and Ferrin, T.E. (2004). UCSF Chimera–a visualization system for exploratory research and analysis. J. Comput. Chem. *25*, 1605–1612. https://doi.org/10.1002/jcc.20084.

67. Wu, N.C., Xie, J., Zheng, T., Nycholat, C.M., Grande, G., Paulson, J.C., Lerner, R.A., and Wilson, I.A. (2017). Diversity of functionally permissive sequences in the receptor-binding site of influenza hemagglutinin. Cell Host Microbe *21*, 742–753.e8. https://doi.org/10.1016/j.chom.2017.05.011.

68. Xu, X., Zhu, X., Dwek, R.A., Stevens, J., and Wilson, I.A. (2008). Structural characterization of the 1918 influenza virus H1N1 neuraminidase. J. Virol. *82*, 10493–10501. https://doi.org/10.1128/JVI.00959-08.

69. Mastronarde, D.N. (2005). Automated electron microscope tomography using robust prediction of specimen movements. J. Struct. Biol. *152*, 36–51. https://doi.org/10.1016/j.jsb.2005.07.007.

70. Shu, Y., and McCauley, J. (2017). GISAID: global initiative on sharing all influenza data - from vision to reality. Euro Surveill. *22*, 30494. https://doi.org/10.2807/1560-7917.ES.2017.22.13.30494.

71. Crooks, G.E., Hon, G., Chandonia, J.M., and Brenner, S.E. (2004). WebLogo: a sequence logo generator. Genome Res. *14*, 1188–1190. https://doi.org/10.1101/gr.849004.

72. Bakan, A., Dutta, A., Mao, W., Liu, Y., Chennubhotla, C., Lezon, T.R., and Bahar, I. (2014). Evol and ProDy for bridging protein sequence evolution and structural dynamics. Bioinformatics *30*, 2681–2683. https://doi.org/10.1093/bioinformatics/btu336.

73. Gao, J., Couzens, L., and Eichelberger, M.C. (2016). Measuring influenza neuraminidase inhibition antibody titers by Enzyme-linked Lectin Assay. J. Vis. Exp.e54573 https://doi.org/10.3791/54573.

74. Leang, S.K., and Hurt, A.C. (2017). Fluorescence-based neuraminidase inhibition assay to assess the susceptibility of influenza viruses to the neuraminidase inhibitor class of antivirals. J. Vis. Exp.e55570 https://doi.org/10.3791/55570.

75. Overdijk, M.B., Verploegen, S., Ortiz Buijsse, A., Vink, T., Leusen, J.H., Bleeker, W.K., and Parren, P.W. (2012). Crosstalk between human IgG isotypes and murine effector cells. J. Immunol. *189*, 3430–3438. https://doi.org/10.4049/jimmunol.1200356.

76. Dekkers, G., Bentlage, A.E.H., Stegmann, T.C., Howie, H.L., Lissenberg-Thunnissen, S., Zimring, J., Rispens, T., and Vidarsson, G. (2017). Affinity of human IgG subclasses to mouse Fc gamma receptors. mAbs *9*, 767–773. https://doi.org/10.1080/19420862.2017.1323159.

STAR★METHODS

KEY RESOURCES TABLE

REAGENT or RESOURCE	SOURCE	IDENTIFIER
Antibodies		
6x-His Tag Monoclonal Antibody (HIS.H8)	Thermo Fisher Scientific	Cat# 14-6657-82
HRP Rat Anti-Mouse Ig, κ Light Chain	BD Biosciences	Cat# 559751
Chemicals, peptides, and recombinant proteins		
Sodium chloride (NaCl)	Fisher Scientific	Cat# S271-500
Hydrochloric Acid, ACS, 12 M	Fisher Scientific	Cat# S25358
Tris Base	Fisher Scientific	Cat# BP152-500
Imidazole	Fisher Scientific	Cat# A10221
Calcium Chloride, Dihydrate	Millipore	Cat# 208291-250GM
DpnI	New England Biolabs	Cat# R0176L
Lipofectamine 2000	Thermo Fisher Scientific	Cat# 11668-019
Cellfectin II Reagent	Gibco	Cat# 10362-100
TPCK-Trypsin	Thermo Fisher Scientific	Cat# 20233
Zanamivir	Sigma-Aldrich	Cat# SML0492
Thrombin	Sigma-Aldrich	Cat# 605157
Coating buffer	KPL	Cat# 50-84-01
2'-(4-Methylumbelliferyl)-α-D-N-acetylneuraminic acid sodium salt hydrate	Sigma-Aldrich	Cat# M8639
Fetuin	Sigma-Aldrich	Cat# F3385
Lectin PNA-HRPO	Sigma-Aldrich	Cat# L7759
Bovine Serum Albumin (BSA)	Fisher Scientific	Cat# BP9706100
Tween 20	Fisher Scientific	Cat# BP337-100
MES monohydrate	Thermo Fisher Scientific	Cat# A16104.22
o-Phenylenediamine dihydrochloride	Sigma-Aldrich	Cat# P8287
Critical commercial assays		
PrimeSTAR Max DNA Polymerase	Takara	Cat# R045A
PureLink PCR Purification Kit	Thermo Fisher Scientific	Cat# K310002
QIAprep Spin Miniprep Kit	Qiagen	Cat# 27106
PureLink HiPure Plasmid Miniprep Kit	Thermo Fisher Scientific	Cat# K210003
Monarch DNA Gel Extraction Kit	New England Biolabs	Cat# T1020L
Deposited data		
NA-1F04 cryo-EM structure	This study	PDB: 8EZ7; EMD-28729
NA-3C08 cryo-EM structure	This study	PDB: 8EZ8; EMD-28730
NA-3A10 cryo-EM structure	This study	PDB: 8EZ3; EMD-28728
Experimental models: Cell lines		
Sf9 cells	ATCC	CRL-1711; RRID: CVCL_0549
MDCK-SIAT1 cells	Sigma-Aldrich	Cat# 05071502-1VL
HEK 293T cells	N/A	N/A
Recombinant DNA		
pHW2000-Mos99 H3N2 HA	This study	N/A
pHW2000-Mos99 H3N2 NA	Lei et al.[32]	N/A
pHW2000-Sing16 H3N2 NA	This study	N/A
WSN eight-plasmid reverse genetics	Neumann et al.[61]	N/A
PR8 eight-plasmid reverse genetics	Neumann et al.[61]	N/A
pFastBac-Bil69 H3N2 NA	Lei et al.[32]	N/A
pFastBac-SD93 H3N2 NA	Lei et al.[32]	N/A

(*Continued on next page*)

Continued

REAGENT or RESOURCE	SOURCE	IDENTIFIER
pFastBac-Mos99 H3N2 NA	Lei et al.[32]	N/A
pFastBac-HK68 H3N2 NA	This study	N/A
pFastBac-Bil71 H3N2 NA	This study	N/A
pFastBac-Alb76 H3N2 NA	This study	N/A
pFastBac-Bk79 H3N2 NA	This study	N/A
pFastBac-Bei89 H3N2 NA	This study	N/A
pFastBac-Wy03 H3N2 NA	This study	N/A
pFastBac-Vic11 H3N2 NA	This study	N/A
pFastBac-Sing16 H3N2 NA	This study	N/A
pFastBac-Kan17 H3N2 NA	This study	N/A
pFastBac-HK19 H3N2 NA	This study	N/A
pFastBac-Can05 H2N2 NA	This study	N/A
pFastBac-NL99 H5N2 NA	This study	N/A
pFastBac-HK97 H9N2 NA	This study	N/A
phCMV3-1F04 IgG heavy chain	This study	N/A
phCMV3-1F04 Fab heavy chain	This study	N/A
phCMV3-1F04 light chain	This study	N/A
phCMV3-3C08 IgG heavy chain	This study	N/A
phCMV3-3C08 Fab heavy chain	This study	N/A
phCMV3-3C08 light chain	This study	N/A
phCMV3-3A10 IgG heavy chain	This study	N/A
phCMV3-3A10 Fab heavy chain	This study	N/A
phCMV3-3A10 light chain	This study	N/A
Software and algorithms		
Octet analysis software 9.0	Sartorius	N/A
R	https://www.r-project.org/	N/A
SAbPred	Dunbar et al.[62]	https://opig.stats.ox.ac.uk/webapps/sabdab-sabpred/sabpred
Phenix suite	Adams et al.[63]	RRID: SCR_014224
Coot	Emsley et al.[64]	RRID: SCR_014222
cryoSPARC	Punjani et al.[65]	https://cryosparc.com; RRID:SCR_016501
UCSF Chimera	Pettersen et al.[66]	http://plato.cgl.ucsf.edu/chimera; RRID:SCR_004097
Other		
Octet analysis software 9.0	Sartorius	N/A
R1.2/1.3 400 mesh Au holey carbon grids	Quantifoil	Cat# 1210627
Octet Anti-Penta-HIS (HIS1K) Biosensors	Sartorius	Cat# 18-5120
Nunc MaxiSorp flat-bottom 96 well plate	Thermo Fisher Scientific	Cat# 44-2404-21
Microplate, 96 Well, PP, F-Bottom	Grenier	Cat# 655209
Sf-900 II SFM	Thermo Fisher Scientific	Cat# 10902088
DMEM medium	Thermo Fisher Scientific	Cat# 11995065
Opti-MEM I Reduced Serum Medium	Thermo Fisher Scientific	Cat# 31985070
GlutaMAX Supplement	Thermo Fisher Scientific	Cat# 35050061
NEAA mixture (100x)	Lonza	Cat# 13-114E
Trypsin-EDTA (0.25%), phenol red	Thermo Fisher Scientific	Cat# 25200056
Penicillin-Streptomycin	Thermo Fisher Scientific	Cat# 15140122
Fetal Bovine Serum (FBS)	Thermo Fisher Scientific	Cat# 16000044
Phosphate-buffered saline (PBS), 1X	VWR	Cat# 21-040-CM
NEB 5-alpha Competent *E. coli*	New England Biolabs	Cat# C2987H

(*Continued on next page*)

Continued

REAGENT or RESOURCE	SOURCE	IDENTIFIER
MegaX DH10B T1R Electrocomp Cells	Thermo Fisher Scientific	Cat# C640003
NA protein sequences	GISAID	http://gisaid.org/
Ni Sepharose excel resin	Cytiva	Cat# 17371202
XK 16/100 Superdex 200 pg	Cytiva	Cat# 90100137

RESOURCE AVAILABILITY

Lead contact

Information and requests for resources should be directed to and will be fulfilled by the lead contact, Nicholas C. Wu (nicwu@illinois.edu).

Materials availability

All plasmids generated in this study are available from the lead contact without restriction.

Data and code availability

- The cryoEM maps and fitted coordinates of Mos99 NA in complex with 3C08, 3A10, and 1F04 Fabs are deposited in the Electron Microscopy Data Bank and Protein Data Bank with accession codes EMD-28730/PDB 8EZ8, EMD-28728/PDB 8EZ3, and EMD-28729/PDB 8EZ7, respectively.
- The heavy and light chain sequences for antibodies 3C08, 3A10, and 1F04 are deposited in GenBank with accession numbers OR602615-OR602620.
- This paper does not report original code.
- Any additional information required to reanalyze the data reported in this paper is available from the lead contact upon request.

EXPERIMENTAL MODEL AND STUDY PARTICIPANT DETAILS

Human materials

All studies were approved by the Institutional Review Board of Washington University in St. Louis. Written consent was obtained from all enrolled participants, who had participated in the previous study.[24] Peripheral blood samples were collected in ethylenediaminetetraacetic acid (EDTA) tubes, and peripheral blood mononuclear cells (PBMCs) were enriched by density gradient centrifugation over Ficoll-Paque PLUS (Cytiva) or Lymphopure (BioLegend). The residual red blood cells were lysed with ammonium chloride lysis buffer, and cells were immediately cryopreserved in 10% dimethyl sulfoxide in fetal bovine serum (FBS).

Cell Lines

HEK 293T cells (human embryonic kidney cells, female) were maintained in DMEM medium (Thermo Fisher Scientific) supplemented with 10% fetal bovine serum (FBS, Thermo Fisher Scientific), 1x MEM non-essential amino acids (Thermo Fisher Scientific), and 100 U mL^{-1} of Penicillin-Streptomycin (Thermo Fisher Scientific). MDCK-SIAT1 cells (Madin-Darby canine kidney cells with stable expression of human 2,6-sialtransferase, female, Sigma-Aldrich) were maintained in DMEM medium supplemented with 10% FBS, 1x MEM non-essential amino acids, and 100 U mL^{-1} of Penicillin-Streptomycin. Sf9 cells (Spodoptera frugiperda ovarian cells, female, ATCC) were maintained in Sf-900 II SFM medium (Thermo Fisher Scientific).

Mice

The animal experiments were performed in accordance with protocols approved by Icahn School of Medicine at Mount Sinai Institutional Animal Care and Use Committee (IACUC). Six-week-old female BALB/c mice (Jackson Laboratory) were used for all animal experiments.

Influenza virus

Recombinant influenza virus was generated based on the A/WSN/33 (WSN) or A/PR/8/34 (PR8) eight-plasmid reverse genetic system.[61] PR8 backbone was used to generate 7:1 reassortants, with the entire neuraminidase (NA) coding region being replaced by those from H3N2 viruses.[67] Transfection was performed in HEK 293T/MDCK-SIAT1 cells (Sigma-Aldrich, catalog number: 05071502-1VL) co-culture (ratio of 6:1) at 60% confluence using Lipofectamine 2000 (Life Technologies) according to the manufacturer's instructions. At 24 h post-transfection, cells were washed twice with phosphate-buffered saline (PBS) and cell culture medium was replaced with OPTI-MEM medium supplemented with 1 $\mu g\ mL^{-1}$ tosyl phenylalanyl chloromethyl ketone (TPCK)-trypsin. Virus was harvested at 72 h post-transfection. For measuring virus titer by the $TCID_{50}$ (median tissue culture infectious dose) assay, MDCK-

SIAT1 cells were washed twice with PBS prior to the addition of virus, and OPTI-MEM medium was supplemented with 1 μg mL^{-1} TPCK-trypsin. Cytopathic effect (CPE) was recorded on day 3 post-infection.

METHOD DETAILS

Cell sorting

Staining for sorting was performed using cryo-preserved PBMCs collected one week after vaccination from one of the participants. The EasySep Human CD4 Positive Selection Kit II (Stemcell) was used to deplete $CD4^+$ T cells. Negative fraction cells were stained for 30 min on ice with CD20-Pacific Blue (2H7, BioLegend, 1:400), IgA-FITC (M24A, Millipore, 1:500), CD38-BB700 (HIT2, BD Horizon, 1:500), CD19-PE (HIB19, BioLegend, 1:200), CXCR5-PE-Dazzle 594 (J252D4, BioLegend, 1:50), IgD-APC (IA6-2, BioLegend, 1:200), CD4-Alexa700 (OKT4, BioLegend, 1:50), IgM-APC-Fire 750 (MHM-88, BioLegend, 1:100), and Zombie Aqua diluted in 2% FBS and 2 mM EDTA in PBS. Cells were washed twice with 2% FBS and 2 mM EDTA in PBS, and single IgM^- IgA^- plasmablasts (live singlet $CD4^-$ $CD19^+$ $CD20^-$ $CD38^+$ IgD^{lo} IgM^- IgA^- $CXCR5^-$) were sorted using a FACSAria II into 96-well plates containing 2 μL Lysis buffer (Clontech) supplemented with 1 U μL^{-1} RNase inhibitor (NEB), and immediately frozen on dry ice.

Expression and purification of Fab and IgG

Heavy and light chains of the antibodies were cloned into phCMV3 plasmids with a mouse immunoglobulin kappa signal peptide in human IgG1 Fc or Fab format. Plasmids encoding the heavy and light chains of antibodies were transfected into Expi293F cells using an ExpiFectamine 293 transfection kit (Gibco) in a 2:1 mass ratio for IgG or a 1:1 mass ratio for Fab following the manufacturer's protocol. Supernatant was harvested 6 days post-transfection and centrifuged at 4000 × *g* for 30 min at 4°C to remove cells and debris. The supernatant was subsequently clarified using a polyethersulfone membrane filter with a 0.22 μm pore size (Millipore). Antibodies were first purified by affinity chromatography, either via the 5 mL HiTrap Protein G HP antibody purification columns (Cytiva) or CaptureSelect CH1-XL beads (Thermo Scientific). Then, the antibodies were further purified by size exclusion chromatography using a HiLoad 16/100 Superdex 200 prep grade column (Cytiva) in PBS. Antibodies were stored at 4°C.

Expression and purification of NA

The NA head domains, which contained residues 82 to 469 (N2 numbering), were fused to an N-terminal gp67 signal peptide, His_6-tag, a vasodilator-stimulated phosphoprotein (VASP) tetramerization domain, and a thrombin cleavage site.[68] Recombinant bacmid DNA that carried the NA ectodomain from the strain of interest was generated using the Bac-to-Bac system (Thermo Fisher Scientific) according to the manufacturer's instructions. Baculovirus was generated by transfecting the purified bacmid DNA into adherent Sf9 cells using Cellfectin reagent (Thermo Fisher Scientific) according to the manufacturer's instructions. The baculovirus was further amplified by passaging in adherent Sf9 cells at a multiplicity of infection (MOI) of 1. Recombinant NA head domains were expressed by infecting 1 L of suspension Sf9 cells at an MOI of 1. On day 3 post-infection, Sf9 cells were pelleted by centrifugation at 4,000 ×*g* for 25 min. Soluble recombinant NA was purified from the supernatant by affinity chromatography using Ni Sepharose excel resin (Cytiva) and then size exclusion chromatography using a HiLoad 16/100 Superdex 200 prep grade column (Cytiva) in 20 mM Tris-HCl pH 8.0, 100 mM NaCl, and 10 mM $CaCl_2$.

ELISA

Assays were performed in MaxiSorp 96-well plates (Thermo Fisher) coated with 100 μL of Flucelvax Quadrivalent 2019/2020 seasonal influenza virus vaccine (Seqirus, 1:100), recombinant HA, NA proteins, or bovine serum albumin at 1 μg mL^{-1} in PBS, and plates were incubated at 4°C overnight. Plates were then blocked with 10% FBS and 0.05% Tween 20 in PBS. Purified recombinant antibodies were diluted to 1 μg mL^{-1} in blocking buffer and added to the plates. Plates were incubated for 90 min at room temperature and then washed 3 times with 0.05% Tween 20 in PBS. Secondary antibodies were diluted in blocking buffer before adding to the wells and incubating for 60 min at room temperature. Horseradish peroxidase (HRP)-conjugated goat anti-human IgG (H+L) antibody (Jackson ImmunoResearch, catalog #: 109-035-088, 1:2,500) was used to detect recombinant antibodies. Plates were washed three times with 0.05% Tween 20 in PBS and three times with PBS before the addition of O-phenylenediamine dihydrochloride peroxidase substrate (MilliporeSigma). Reactions were stopped by the addition of 1 M hydrochloric acid. Optical density was measured at 490 nm.

Biolayer interferometry binding assay

Binding assays were performed by biolayer interferometry (BLI) using an Octet RED96e instrument (Sartorius). Briefly, His_6-tagged NA protein at 20 μg mL^{-1} in 1x kinetics buffer (1x PBS, pH 7.4, and 0.002% Tween 20) was loaded onto nickel-nitrilotriacetic acid (Ni-NTA) biosensors and incubated with 200 nM, 100 nM, 50 nM, and 25 nM of Fabs. The assay consisted of five steps: 1) baseline: 60 s with 1x kinetics buffer; 2) loading: 120 s with His_6-tagged NA protein; 3) baseline: 60 s with 1x kinetics buffer; 4) association: 60 s with Fabs; and 5) dissociation: 60 s with 1x kinetics buffer. For estimating the K_D, a 1:1 binding model was used. In cases where the binding affinity was relatively weak (K_D > 100 nM), a 1:1 binding model did not fit well due to the contribution of non-specific binding to the response curve. Subsequently, a 2:1 heterogeneous ligand model was used to improve the fitting. "No binding" was defined as maximum response of less than 0.05 or 2:1 fitting mode with R^2 less than 0.98.

Cryo-EM sample preparation, data collection, and data processing

The purified NA protein was mixed with each Fab and incubated on ice overnight before size exclusion chromatography. The peak fraction of the Fab-NA complex was concentrated to around 1 mg mL^{-1} for cryo-EM sample preparation. Cryo-EM grids were prepared using a Vitrobot Mark IV machine. An aliquot of 3.5 μL sample was applied to a 300-mesh Quantifoil R1.2/1.3 Cu grid pretreated with glow-discharge. Excess liquid was blotted away using filter paper with blotting force -5 and blotting time 3 s. The grid was plunge frozen in liquid ethane. Data collection was done with serialEM[69] on a Titan Krios microscope equipped with Gatan BioQuantum K3 imaging filter and camera. A 10 eV slit was used for the filter. Images were recorded at 130,000x magnification, corresponding to a pixel size of 0.53 Å/pix at super-resolution mode of the camera. A defocus range of -0.8 μm to -1.5 μm was set. A total dose of 50 $e^-/Å^2$ of each exposure was fractionated into 50 frames. The first two frames of the movie stack were excluded in motion-correction. Cryo-EM data processing was performed on the fly with cryoSPARC Live,[65] following regular single-particle procedures.

Model building and refinement

For model building, we used ABodyBuilder-ML of the SAbPred web server[62] to generate an initial model for each Fab. This model, together with the model of NA (PDB 7U4F),[32] was fitted into the cryo-EM density map using UCSF Chimera.[66] The models were manually adjusted in Coot[64] and refined with Phenix real-space refinement program.[63] This process was iterated for several cycles until no significant improvement of the model was observed.

Sequence conservation analysis

A total of 66,562 full-length human H3N2 NA protein sequences from different subtypes were downloaded from the Global Initiative for Sharing Avian Influenza Data (GISAID; https://gisaid.org).[70] To avoid temporal sampling bias, we sampled at most 10 sequences per year, which resulted in a total of 498 NA sequences. Sequence logos were generated by WebLogo.[71] Sequence entropy was calculated by Evol, a package in Prody.[72] Sequence conservation score of a residue i was computed from its sequence entropy by:

$$\textit{Sequence conservation score}_i = \left(1 - \frac{\textit{entropy}_i - \textit{entropy}_{min}}{\textit{entropy}_{max} - \textit{entropy}_{min}}\right) \times 100$$

where $entropy_{max}$ and $entropy_{min}$ represent the maximum and minimum entropy values across all residues, respectively. Thus, the sequence conservation score was normalized to a range of 0 to 100, where more conserved residues would have a higher sequence conservation score.

Enzyme-linked lectin assay (ELLA)

ELLA experiments were performed described.[73] Briefly, each well of a 96-well microtiter plate (Thermo Fisher) was coated with 100 μL fetuin (Sigma) at 25 μg mL^{-1} in coating buffer (KPL coating solution; SeraCare) at 4°C overnight. The next day, 50 μL antibodies antibodies at the indicated concentrations in 2-(N-morpholino)ethanesulfonic acid (MES) at pH 6.5, 20 mM $CaCl_2$, 1% bovine serum albumin and 0.5% Tween 20 were mixed an equal volume of NA (0.032 μg/well). This mixture was added to the fetuin-coated plate and incubated for 18 h at 37°C. The plate was then washed six times with PBS with 0.05% Tween 20. Subsequently, 100 μL of HRP-conjugated peanut agglutinin lectin (PNA-HRPO, Sigma–Aldrich) in MES at pH 6.5 with $CaCl_2$ and 1% bovine serum albumin was added and incubated for 2 h at room temperature in the dark. The plate was washed six times and developed with 3,3'5,5'-tetramethylbenzidine (TMB) ELISA substrate (Sigma). Absorbance was read at 450 nm using a SpectraMax M2 microplate reader (Molecular Devices). Data points were analyzed using Prism software and the 50% inhibition concentration (IC_{50}) was defined as the concentration at which 50% of the NA activity was inhibited compared to the negative control.

MUNANA assay

Our protocol was adopted from a previous study.[74] Briefly, 120 ng of recombinant NA was incubated with the indicated antibody at 37°C for 1 h in a 96-well half area plate (Corning), then with 100 μM 2′-(4-methylumbelliferyl)-α-d-N-acetylneuraminic acid (MUNANA) in PBS that contained 33 mM MES pH 6.5 and 4 mM $CaCl_2$ for an additional 1 h. After adding the stop solution (138 mM NaOH in ethanol), the relative fluorescence unit (RFU) was measured by a BioTek Synergy HTX Multimode Reader (Agilent) with an excitation at 360 nm and an emission at 460 nm. The RFU of each sample was normalized to that of the negative control with no antibody. The normalized RFU was reported as the relative NA activity.

Virus growth inhibition assay

Madin-Darby canine kidney (MDCK) cells were seeded in a 96-well, flat-bottom cell culture plate (Thermo Fisher). The next day, serially diluted antibodies or zanamivir were mixed with an equal volume of virus and incubated at 37°C for 1 h. The antibody/virus mixture was then incubated with the MDCK cells at 37°C after the cells were washed twice with PBS. After 1 h incubation, the antibody/virus mixture was replaced with Minimum Essential Medium (MEM) supplemented with 25 mM of 4-(2-hydroxyethyl)-1-piperazineethanesulfonic acid (HEPES), 1 μg mL^{-1} of Tosyl phenylalanyl chloromethyl ketone (TPCK)-trypsin, and antibodies at the same concentration as the initial incubation. The plate was incubated at 37°C for 72 h and the presence of virus was detected by hemagglutination assay. The results were analyzed using Prism software.

ADCC reporter bioassay

1.5 x 10^4 MDCK cells were seeded in white, flat bottom 96-well cell culture plates (Thermo Fisher) and incubated at 37°C overnight. The next day, cells were washed three times with PBS and 100 μL of recombinant influenza virus at 1.5 × 10^6 plaque forming units (PFU) mL^{-1} in MEM was added to each well. After incubating the plate for 24 h at 37°C, the media was removed and 25 μL of serially diluted antibodies in 1:10 in Roswell Park Memorial Institute (RPMI) 1640 media (Thermo Fisher), 25 μL of effector cells (engineered Jurkat cells stably expressing human FcγRIIIa V158 and NFAT-induced luciferase) and 25 μL of RPMI 1640 media were added. After 6 h incubation at 37°C, 75 μL of Bio-Glo luciferase (Promega) was added to each well. The plate was incubated for 10 min in the dark and the luciferase induced luminescence measured with a BioTek Synergy HTX Multimode Reader (Agilent). Data were analyzed using Prism software and the area under the curve (AUC) values were determined.

Prophylactic and therapeutic protection experiments

Female BALB/c mice at 6 weeks old (n = 5 mice/group) were anesthetized with a ketamine/xylazine/water mixture and intranasally infected with 5 × median lethal dose (LD_{50}) of recombinant N2/Mos99 virus or N2/Sing16 (7:1 on backbone from A/Puerto Rico/8/1934). Mice were given the indicated antibody at a dose of 5 mg/kg intraperitoneally at 2 h before infection (prophylaxis) or 72 h after infection (therapeutics). Weight loss was monitored daily for 14 days. The humane endpoint was defined as a weight loss of 25% from initial weight on day 0. Of note, while our BALB/c mice were not modified to facilitate interaction with human IgG1, human IgG1 could interact with mouse Fc gamma receptors.[75,76] To determine the lung viral titers, lungs of infected mice were harvested and homogenized in 1 mL of MEM with 10% bovine serum albumin using a PowerLyzer 24 Homogenizer (Qiagen). Subsequently, virus titers were measured by $TCID_{50}$ (median tissue culture infectious dose) assay. The results were analyzed using Prism software.

QUANTIFICATION AND STATISTICAL ANALYSIS

Standard deviation for K_D estimation was computed by Octet analysis software 9.0. Wilcoxon rank sum test and Student's t-test were performed in R.